This is a non-peer-reviewed preprint submitted to EarthArXiv
This manuscript has been submitted to Marine Geology for peer review

EARLY PLIOCENE DRAWDOWN AND EXPANSION OF THE ANTARCTIC PENINSULA ICE SHEET IN MARGUERITE BAY

Sandra Passchier[1*], Ridley Joseph[1], Monika Ghimire[1], Xiaona Li[1]

[1]Department of Earth and Environmental Studies, Montclair State University, 1 Normal Ave, Montclair, NJ, U.S.A.

[*]Corresponding author: passchiers@montclair.edu

ABSTRACT

The Antarctic Peninsula Ice Sheet (APIS) is situated in a rapidly and persistently warming region of Antarctica and its behavior under warmer conditions projected for Earth's future remains poorly constrained. Interpretations of stratigraphic records of ice-sheet change from periods of warmth in Earth's past are essential in providing boundary conditions for estimates of future ice loss and its climate feedbacks. The early Pliocene exhibited surface temperatures that were 3-4 °C higher than present under similar greenhouse forcing. Here we present new sedimentological and geochemical data from the early Pliocene section recovered in Ocean Drilling Program Site 1097 to assess the effects of atmospheric and ocean warming on ice extent and glacial regime. The reconstruction of Pliocene glacial processes and sediment provenance within an updated chronology of Site 1097, indicates that ice was absent from the Marguerite Bay with supply from local glaciers only at ~5.2 to 4.8 Ma. A subsequent shift in sediment provenance suggests that the APIS began to dominate ice drainage into Marguerite Bay ~4.5 Ma with the sedimentology of the deposits pointing to a subpolar, meltwater-intensive glacial system before ~4.3 Ma. In contrast, a massive and stratified diamictite-dominated section younger than ~4.3 Ma, shows characteristics similar to Pleistocene deposits from the Marguerite Ice Stream Trough. These changes in sedimentary systems reflect enhanced accumulation and retreat phases of the terrestrial Antarctic Peninsula Ice Sheet under Pliocene peak warming and stable marine ice-sheet growth upon cooling, providing critical insights into the dynamics of this ice sheet in response to sustained warmth.

KEY WORDS

Antarctic Peninsula; Marine sediment; Pliocene; Grain size; Geochemistry; Provenance; Ice sheet

1. INTRODUCTION

1.1. Background

The response of polar marine ice sheets to future warming is an area of great uncertainty in sea-level projections. Marine ice-sheets with ice shelves are vulnerable to both atmospheric and ocean warming creating complexity in response scenarios and numerical modeling. Surface melt in response to atmospheric warming creates pools of freshwater on top of an ice shelf that can weaken the floating ice slab through hydrofracturing while ocean warming thins an ice shelf through basal melt (Vaughan, 2006; Pritchard et al., 2012). However, over millennial timescales feedbacks related to precipitation and snow accumulation, basal melt, reduced sea ice, and glacio-isostatic rebound may stabilize marine-grounded portions of ice sheets (Kingslake et al., 2018). Ice-proximal sediment records spanning several glacial-interglacial cycles are used to observe long-term behavior of marine ice-sheet and changes in glacial regime under sustained warmth.

Today outlet glaciers on the southwestern margin of the Antarctic Peninsula Ice Sheet (APIS) are buttressed by the George VI Ice Shelf, a 100 to 600-m thick slab of ice covering the channel between Alexander Island and Palmer Land (Figure 1). For the past few decades, the George VI Land ice shelf has retreated and exhibited surface melt and excessive thinning (Holt et al., 2013; Davies et al., 2017; Smith et al., 2020). The George VI ice shelf is affected by incursions of CDW from the Bellingshausen Sea and experiences basal melt with meltwater being evacuated at its northern front into Marguerite Bay (Jenkins and Jacobs, 2008). Due to the proximity of modern ocean frontal systems to the southern Antarctic Peninsula, the impact of changes in the wind-driven circulation on CDW incursions, ocean heat transport and ice-shelf stability are a major concern (Lamy et al., 2023). While the effect of rising air temperatures on ice-shelf integrity is well-documented from the instrumental record (e.g., Scambos et al., 2004; Cook et al., 2005), the effects of changes in ocean circulation and advection of warm circumpolar deepwater (CDW) towards the continental shelf are more difficult to monitor. Modeling studies suggest that the George VI ice shelf, the second largest ice shelf on the Antarctic Peninsula, will be one of the least viable by 2100 putting the APIS at risk of accelerated mass loss (Burgard et

al., 2025). Notably, the nearby Wordie ice shelf of the APIS in Marguerite Bay has already disintegrated with acceleration of upstream conduits that converge into the Fleming Glacier since the 1980s (Friedl et al., 2018).

Early Holocene paleorecords from George VI Sound and the nearby Amundsen Sea provide long-term context to short-term modern observations and establish a connection between sub-ice shelf basal melt, ice-shelf collapse and ice retreat in response to incursions of CDW (Smith et al., 2007; Hillenbrand et al., 2017). Based on correlations between Holocene paleorecords, ocean forcing of the basal ice-shelf melt and ice-shelf collapse were attributed to systemic changes in wind-driven circulation in the Southern Ocean. While the George VI ice shelf was absent during the warm early Holocene, it reformed rapidly under conditions of early Holocene climate cooling (Smith et al., 2007). However, the Holocene is an imperfect analogue for future conditions with expected higher than pre-industrial greenhouse gas concentrations in the atmosphere, more intense warming, and different high-latitude feedbacks (Fox-Kemper et al., 2021). Therefore, gaining a better understanding of pre-Quaternary ice behavior on the Antarctic Peninsula and its drivers is crucial because, in contrast to the Pleistocene and Holocene, Earth's climate system exhibited configurations that are more comparable to future climate scenarios (Davies et al., 2012).

1.2. Antarctic paleoclimate and ice-sheet history

The early Pliocene was the warmest period in the past 5 Million years (Myrs) with surface temperatures more than 4.8 °C higher than pre-industrial under similar to present greenhouse forcing (Fedorov et al., 2013; Tierney et al., 2025). Early Pliocene Antarctic warm events with reduced sea-ice were previously detected in marine sediment archives in the Indian Ocean sector of Antarctica using silicoflagellate-based sea surface temperature (SST) records (Whitehead and Bohaty, 2003, 2005) and as elevated biogenic opal content in continental rise sediments in the Bellingshausen Sea (Hillenbrand and Ehrmann, 2005). Furthermore, ice-sheet retreat during these early Pliocene warm events allowed for open marine conditions and the deposition of diatomite in the Ross Sea, an embayment on the Pacific Ocean side (Naish et al., 2009). Following the early Pliocene climatic optimum South Pacific and Antarctic ocean temperatures cooled (Karas et al., 2011; McKay et al., 2012). The imprint of Northern Hemisphere ice sheets

on the global climate system increased from ~4 Ma in response to bipolar feedbacks as suggested by analyses of stable isotope proxies of ice volume (Westerhold et al., 2020; Clark et al., 2025).

Glaciation on the Antarctic Peninsula, with modern topography extending to more than 3000m in elevation, began in the Eocene as terrestrial glaciers and ice caps (Anderson et al., 2011; Davies et al., 2012). In the southern Antarctic Peninsula, on Alexander Island (Figure 1), sub-ice volcanic eruptions took place in the late Miocene ~7.7-5.4 Ma signaling the presence of local ice caps (Smellie et al., 2009). Off the northern Antarctic Peninsula, a marine sedimentary and pollen record on the Weddell Sea side indicated glacial intensification with ice overriding beginning in the early Pliocene (Anderson et al., 2011). Surface exposure dating of bedrock onshore implied the presence of a sliding glacial ice cover from about 4.69 Ma (Johnson et al., 2009), even though the location of the exposure surfaces that were dated, as well as fossil and volcanic rock evidence, suggested that the early Pliocene ice cover was thin and did not exceed 200 m in thickness (Smellie et al., 2009). The timing of the transition of the APIS from a thin ice sheet with multiple ice centers into a fully coalesced ice sheet with ice advances across the continental margin is poorly known.

The record of the early Pliocene phases of warming and the glacial intensification and ice-sheet advance onto the continental shelf that followed is poorly studied in West Antarctic marine sediment paleoarchives, especially on the Pacific margin. Here we investigate the paleoglaciology of the APIS in Marguerite Bay through the early Pliocene warm period and cooling through new data collection at a legacy Ocean Drilling Program (ODP) drillsite, Site 1097, on the George VI Land continental shelf (Shipboard Scientific Party, 1999)(Figure 1).

1.3. Geology of study area

The George VI Sound upstream from the Marguerite Trough separates the Central Domain of the Antarctic Peninsula in Palmer Land from the Western Domain in Alexander Island (Burton-Johnson and Riley, 2015)(Figure 2). Northwestern Palmer Land is underlain primarily by Jurassic and younger basaltic-andesitic-rhyolitic arc-volcanic rocks overlying metamorphic basement and plutonic rocks that are exposed on the east coast of George VI Sound and in eastern Marguerite Bay. White granites, banded gneisses and amphibolites make up the metamorphic basement, and are intruded by felsic to intermediate plutonic rocks of the Late-Jurassic-Cretaceous Antarctic Peninsula Batholith and the Palmer Land and Antarctic Peninsula

Volcanic Group rocks (Davies, 1984; Smith, 1987; Leat et al., 2009). Rock clasts in recent glacial sediments on the margin of George VI Sound interpreted to be sourced from western Palmer Land include foliated amphibolite and felsic gneiss, coarse-grained granitic and quartz-rich dioritic lithologies, as well as dacite-rhyolitic and basaltic-andesitic volcanic rocks (Davies et al., 2017). Overcompacted diamictons sampled in the trough in Marguerite Bay contain pebbles of predominantly schists and gneisses with minor mafic/intermediate volcanics, felsic/intermediate plutonics, amphibolite and metavolcanics, whereas mafic/intermediate volcanics and felsic/intermediate plutonics dominate in glaciomarine sediments across Marguerite Bay (Kennedy and Anderson, 1989).

Most of Alexander Island west of the LeMay fault is underlain by the LeMay Group, a predominantly Mesozoic accretionary complex of weakly metamorphosed volcaniclastic rocks (Figure 2) with embedded fragments of allochthonous oceanic basalts (Doubleday et al., 1994, Willan, 2003; Riley et al., 2023). In addition, rocks east of the LeMay Fault consist of a narrow band of sedimentary and metasedimentary rocks of the Fossil Bluffs Group that originated in a Jurassic-Cretaceous fore-arc basin and today extend into the graben of the George VI Sound (Crame and Howlett, 1988; Constantino et al., 2020). The George VI Sound is a graben structure that developed in the Late Cretaceous-Early Cenozoic through tectonic inversion within the Mesozoic accretionary complex (Doubleday and Story, 1998). Cretaceous-Paleogene basaltic-andesitic-rhyolitic arc-volcanic rocks 2000 m in thickness unconformably overlie the LeMay Group accretionary complex in an upland plateau, the Elgar Uplands, in the center of Alexander Island (Figure 2)(McCarron and Smellie, 1998; Riley et al., 2023). Neogene alkaline basalts in turn overlie the Cretaceous-Paleogene arc-volcanics, but are more widespread to the west of Alexander Island (Hole, 1988, 1990, 1993). Clasts sourced from Alexander Island in recent glacial sediments on the margin of the George VI Sound include well-rounded lava pebbles, sorted arkoses and lithic sandstones, with some exhibiting evidence of contact-metamorphism (Davies et al., 2017).

Adelaide Island, which is covered with a piedmont glacier at its northwestern side, is considered to be part of the same Mesozoic fore-arc complex as Alexander Island (Riley et al., 2012). Exposed rocks are Mesozoic volcaniclastic sediments, sandstones and conglomerates that are correlative to the Fossil Bluff Group of Alexander Island, and Late Cretaceous-Paleogene

basalts, minor rhyolites, and granodiorite, tonalite and granodiorite-gabbro hybrid plutons (Riley et al., 2012). Eroded fore-arc volcanics and sediments are possibly also present in a mid-shelf high upstream from Site 1097 (Larter et al., 1997; Bart et al., 2005)(Figure 3).

2. METHODS AND MATERIALS

2.1. Site 1097

The George VI Land continental shelf is approximately 500 m deep at the shelf edge with water depths increasing to 1500 m landward in the Marguerite Ice Stream Trough (Ó Cofaigh et al., 2005). The modern trough is about 50–80 km wide and 370km long and crosses the shelf from the mouth of George VI Sound through Marguerite Bay to the edge of the continental shelf (Figure 1). A cross-shelf trough first developed to the southwest of the Marguerite Trough and migrated to its present position in the Pliocene (Bart et al., 2005; Hernández-Molina et al., 2017)(Figure 3). Ocean Drilling Program (ODP) Site 1097 was drilled on the George VI Land outer continental shelf in 551.7 meters water depth and reached 436.6 meters below seafloor (mbsf). It is positioned about 14 km landward from the shelf break near the mouth of the modern Maguerite Trough, and on northeast flank of the paleotroughs (Shipboard Scientific party, 1999; Bart et al., 2005)(Figure 3).

2.2 Lithology and stratigraphic correlations

Upon shipboard core description at Site 1097 three main lithofacies were recognized: 1) massive diamictite, 2) graded and stratified diamictite and 3) mud (Shipboard Scientific Party, 1999; Eyles et al., 2001). Below ~150 mbsf interstratified, diamictite, gravel and mud facies with common deformation features and better preserved marine microfaunas represent intermittent open marine conditions and sediment gravity flows (Eyles et al., 2001). Interpretations of diatom taxa below ~150 mbsf suggest that the shelf paleobathymetry was shallower than it is today (Bart and Iwai, 2012). While sediments between ~150 and 180 mbsf were poorly recovered at Site 1097 and consisted mainly of washed gravel (Shipboard Scientific Party, 1999), the upper ~150 mbsf were characterized as massive diamictites originating from glaciomarine deposition and subsequent subglacial reworking and deformation with poorly preserved marine microfossils (Eyles et al., 2001). Reworked and in situ diatoms in this interval show evidence of intermittent glacial retreat on an overdeepened continental shelf (Bart and Iwai, 2012).

Bart et al. (2005) correlated the recovered sediments below ~180 mbsf at Site 1097 to the upper part of a regionally defined seismic unit, Seismic Package 3, and the recovered sediments above ~180 mbsf to the overlying Seismic Package 2 (Figure 3). In Seismic Package 3 individual seismic units are discontinuous with cross-cutting unconformities, and mapped troughs do not exhibit clear cross-shelf geometries (Bart et al., 2005). In contrast to Seismic Package 3 with semi-aggradational stratal stacking, Seismic Package 2 exhibits clinoforms displaying more than 2-3 km of upper slope progradation (Larter et al., 1997; Bart and Iwai, 2012). The base of Seismic Package 2 is correlative to a core depth of ~180 mbsf at Site 1097 (Bart et al., 2005).

2.3 New data collection and data integration

We build upon these earlier studies by conducting a detailed sedimentological investigation with collection of instrument data that enhances the understanding of APIS change through the early Pliocene climate transitions. We also update the chronology of the paleoarchive and reconstruct ice sources and glacial regime of APIS using new particle size and geochemical results. We target the Pliocene interval between ~80 and 343 mbsf; above ~80 mbsf core recovery was too low for meaningful stratigraphic studies, whereas age control was insufficient below ~343 mbsf. Shipboard core descriptions show considerable heterogeneity in facies distributions downcore (Shipboard Scientific Party, 1999), which we explore using new particle size data sets. Clast lithologies for clasts > 0.5 cm diameter were determined shipboard for most cores at Site 1097. Lithologies include volcanics, such as basalt, volcaniclastics, andesite, rhyolite, mafic to felsic plutonic igneous rocks, including granite and diorite, and metamorphic rocks (Shipboard Scientific Party, 1999). For this study, clast counts were normalized by meter of core recovered to assess changes in clast abundance and lithology downcore. Coarse fraction and matrix of diamictites may not always detect the same source due to differences in the mechanical durability of rock clasts and minerals in glacial transport leading to grain-size partitioning of minerals, even in the absence of hydrodynamic sorting. Thus, sediment provenance is interpreted using the clast lithology in conjunction with new bulk geochemical results (this study) from the matrix of the sediments. The sampling strategy was designed to capture lithofacies transitions in the recovered core and a total of 42 samples were collected and analyzed.

2.3.1 Grain-size analysis

Grain-size analysis was carried out on all 42 samples. Approximately 0.5 cc of drill-core sample was placed in a 250-ml beaker. Circa 10 ml of 30% hydrogen peroxide solution was added to remove organic material present in the sediment, and Millipore water was added until the volume reached approximately 50 ml. The contents of the beaker were swirled to promote sediment disaggregation and then heated on a hot plate. After the reaction ceased, hydrochloric acid was added to dissolve calcium carbonate, and the beakers were removed from the hot plate once all chemical reactions ceased. The beakers were then cooled, and the samples were transferred to a 50-ml centrifuge tube and spun at 2000 rpm for 30 minutes. The supernatant was removed, the tubes were refilled with Millipore water, and the centrifuge process was repeated. Before transfer to the instrument, samples were transferred back to the 250-ml beakers, manually disaggregated and heated with Sodium Pyrophosphate to chemically disperse clay aggregates. Samples were measured on a Malvern Mastersizer 3000 laser particle sizer at Montclair State University using a standard operating protocol for Sediments defined in Passchier (2025).

2.3.2 Bulk geochemistry

Bulk geochemical analysis of the matrix was carried out on 39 samples. For ICP-MS sample preparation was modified from Murray et al. (2000). Samples, with gravel pieces removed, were ground to a fine powder with an alumina mortar and pestle. Approximately 100mg of sample was weighed, and fused with lithium metaborate flux in a furnace at 1050 °C. The glass beads were digested in 50ml of 7% nitric acid. Immediately prior to measurement on the ICP-MS, 0.5 ml of the master solution was pipetted into a tube with 9.5 ml of 2% nitric acid solution to achieve a dilution factor of 10,000x. Twelve United States Geological Survey rock standards were prepared using the same method and 10 of these standards were used for generating calibration lines for each element, whereas the standards MAG-1 and SCO-1 were used to check accuracy. Samples were measured on a Thermo Scientific iCap Q ICP-MS at Montclair State University.

3. SEDIMENTOLOGY

Integrating visual core descriptions and core images (Shipboard Scientific Party, 1999)(Figure 4) with new grain-size data (this study), we subdivide the stratigraphy between 80 and 350 mbsf into Lithostratigraphic Units and characterize facies assemblages within these Lithostratigraphic Units down core (Figure 5).

234 3.1. Lithostratigraphic Unit 1 (LSU 1)

235 3.1.1. Massive and stratified diamict

236 Between 80 and 151 mbsf, the sedimentary sequence consists of ~20-25-m thick intervals of
237 massive clast-rich to clast-poor diamictite, alternating with stratified clast-rich diamictite with
238 wispy silt or sand laminae, diatom-rich laminae or horizontal and low-angle bedding (Shipboard
239 Scientific Party, 1999)(Figure 5). Grain-size distributions of the sediments show that massive
240 diamictites in this interval generally exhibit a uniform grain-size distribution with a fine-silt
241 mode and up to 20% sand component in the matrix (< 2mm), whereas stratified diamictites
242 exhibit a more variable sand-silt percentage and typically a higher clay content than massive
243 diamictites (Figures 3).

244 3.1.2. Interpretation

245 The massive and stratified diamictites in LSU 1 resemble sediment facies of modern and ancient
246 ice-shelf depositional environments (Kennedy and Anderson, 1989; Evans and Pudsey, 2002; Ó
247 Cofaigh et al., 2005; Smith et al., 2019), with deposition and reworking in subglacial or ice-
248 contact environments (Eyles et al., 2001). Grain-size distributions of massive diamictons that are
249 uniform are consistent with subglacial processes of sediment generation (Kennedy and Anderson,
250 1989; Prothro et al., 2018). However, distinguishing between massive diamictites that originated
251 in subglacial vs. proglacial glaciomarine environments without geomorphological context is not
252 straightforward (Licht et al., 1999; Passchier et al., 2003). In contrast, the stratified diamictites
253 with wispy silt and sand laminae, diatomaceous laminae, and grain-size distributions showing
254 variability in sand and silt content, more convincingly indicate deposition seaward of the
255 grounding zone (Kennedy and Anderson, 1989). Previous work showed that the diamictite matrix
256 also contains a minor diatom component and fragments as well as sediment-filled and discolored
257 tests of reworked benthic foraminifera, molluscs, sponge spicules, and echinoderm spines
258 (Shipboard Scientific Party, 1999; Eyles et al., 2001). The presence of reworked and abraded
259 foraminifera supports an interpretation of subglacial deformation of previously deposited
260 proglacial sediments, glacigenic debris flows, and currents that are associated with the
261 development of grounding zone wedges (Eyles et al., 2001; Prothro et al., 2018).

262 3.2. Lithostratigraphic Unit 2 (LSU 2)

263 3.2.1. Interstratified diamict, mud with dispersed clasts, laminated mud, sand and gravel

264 The interval between 151 and 179 mbsf is poorly recovered and consists mainly of washed
265 gravel. Below it, between 179 and 218 mbsf, the formation consists of weakly fissile, stratified
266 or banded diamictite and pebbly mud interbedded with gravel, sand, and mud on a cm- to dm-
267 scale (Shipboard Scientific Party, 1999). Bioturbated and laminated diatom bearing muds were
268 recovered as part of this unit and diatomaceous intraclasts are also present. Inclined bedding and
269 other forms of syn-sedimentary deformation were observed, and normal and reverse graded
270 diamictite and gravel is also present (Shipboard Scientific Party, 1999). Grain-size distributions
271 of the matrix of the LSU 2 sediments show a dominance of clayey silt with a small up to 10%
272 sand component at the bottom of the unit, and fine sandy silt at the top of the unit in a sample
273 from stratified diamictite with deformed sand-silt bedding (Figure 4).

274 3.2.2. Interpretation

275 The fine-grained and sorted character of the matrix dominated by clayey silt, and the banding
276 and stratification could be indicative of deposition from meltwater plumes (Lepp et al., 2022).
277 Massive and graded interbeds of gravel and sand indicate more proximal positions to the point
278 source of meltwater discharge, fluctuations in discharge, and gravity flow. Foraminiferal
279 assemblages point to a glaciomarine environment with freshwater input as well (Shipboard
280 Scientific Party, 1999). In contrast, laminated and bioturbated diatomaceous mud beds without
281 gravel probably represent ice-distal conditions and diatomaceous mud intraclasts are likely
282 reworked from similar beds. The interstratified clast-bearing deposits represent periods of
283 hemipelagic deposition with iceberg rafting. Inclined bedding, syn-sedimentary deformation, and
284 graded bedding indicate gravity instability, which was likely facilitated by the high water content
285 of the interstratified fine-grained and diatomaceous hemipelagic sediments.

286 Diatomaceous muds with a negligible ice rafted component dominate the current interglacial
287 sediments in deep shelf basins of Marguerite Bay (Kennedy and Anderson, 1989) and laminated
288 muds and sands, interpreted as meltwater plumites have been observed in subseafloor sediments
289 of the nearby Amundsen Sea (Lepp et al., 2022). However, although subglacial meltwater
290 channels up to 200 m deep are found incised into bedrock on the inner to middle George VI Land
291 continental shelf, associated coarse-grained meltwater deposits have not been detected in shallow
292 drillcores of the Marguerite Trough (Kennedy and Anderson, 1989; Ó Cofaigh et al., 2005). The

coarse grained and laminated facies within LSU 2 also resemble those of more temperate maritime glaciers which include sand and gravel rich meltwater-sorted facies, such as those adjacent to the Gulf of Alaska (Gustavson and Bootroyd, 1987; Powell and Molnia, 1989).

3.1. Lithostratigraphic Unit 3 (LSU 3)

3.3.1 Massive clast-rich diamict

The massive diamictites present between ~219 and 276 mbsf (Cores 27R-33R) are clast-rich with variation in matrix grain-size from sandy to muddy (Figure 4). Boulder and cobble diamictites with clasts up to 40 cm occur at the top of the interval above a sequence that was poorly recovered as washed gravel between ~236 and 265 mbsf (Shipboard Scientific Party, 1999)(Figure 5). The clast-rich massive diamictite below the interval of poor recovery, below ~265 msbf, has pebble-sized clasts and a fine-grained silty clay matrix (Shipboard Scientific Party, 1999).

3.3.2. Interpretation

The massive clast-rich diamictites of LSU 3 were probably deposited in an ice-proximal glaciomarine environment. Reworked poorly preserved benthic foraminifera were found in this unit as well and support an interpretation of subglacially transported sediment (Eyles et al., 2001). However, calcareous nannofossils of the genus *Dictyococcites* found within the interval with the very large boulder and cobble-sized clasts at the top of LSU 3 indicate open marine conditions (Iwai et al., 2001). In this context the large boulders may originate by calving of large icebergs dumping supraglacial and interglacial debris upon retreat of a marine ice-sheet that was grounded on the outer continental shelf (Evans and Pudsey, 2002).

3.4. Lithostratigraphic Unit 4 (LSU 4)

3.4.1. Interstratified diatom-bearing mud with clasts, diamictite and laminated silt

The interval between 284 and 296 mbsf comprises of bioturbated diatom-bearing sandy mud with dispersed clasts interbedded on a dm-to m-scale with diamictite and uniform to finely laminated mud that does not include dispersed clasts. The bedding is intensely deformed, commonly steeply inclined with soft-sediment folding of the finely laminated mud. Mollusk fragments are present as well (Shipboard Scientific Party, 1999). Grain-size distributions of the

different facies range from a moderately sorted coarse sandy silt or silty sand for the matrix of the interbeds with clasts, whereas the uniform or finely laminated facies is a clayey silt (Figure 4).

3.4.2. Interpretation

Sediment facies similar to the dominant facies of bioturbated sandy mud with dispersed clasts with diamictite interbeds In LSU 4 are found near or beyond the calving zone of ice shelves or in the absence of ice shelves on the modern Antarctic continental shelf (O' Cofaigh et al., 2005; Prothro et al., 2018; Smith et al., 2019). Previous work indicated the presence of sparse to abundant benthic foraminifera in isolated beds in LSU 4 with species characteristic of the modern Antarctic outer continental shelf in water depths < 500 m (Eyles et al., 2001). However, diatom evidence suggests that the continental shelf was shallower than today (Bart and Iwai, 2012). The coarse material in this facies was likely deposited after rain-out from icebergs as they melted, with isolated diamictite interbeds representing more intense periods of ice rafting and iceberg dump structures. The soft-sediment deformation of the strata could be due to iceberg ploughing or gravity instability. The sorting of the matrix into a sandy silt or silty sand reflects currents that operated to sort glaciogenic sediments as they settled through the water column (McCave and Andrews, 2019) or by winnowing of sediments shortly after deposition. In addition to the ice-rafted and winnowed sediment facies, the interbeds of moderately sorted uniform and laminated silt without gravel in LSU 4 can be interpreted as meltwater plumites that were deposited when currents moved slowly. These types of deposits have been found to at least 250 km seaward of the grounding line on modern Antarctic continental shelves in association with ice-rafted sediments (Prothro et al., 2018; Lepp et al., 2022).

3.5. Lithostratigraphic Unit 5 (LSU 5)

3.5.1. Bioturbated mud with dispersed clasts

Sediments between 303 and 309 mbsf (Core 36R) are characterized as intensely bioturbated sandy mud with dispersed pebbles. Some cm-scale interbeds of diamictite are also recognized. Grain-size data show a uniform moderately to well-sorted distribution downcore with a distinct mode in the very coarse silt to fine sand range and a fine tail (Figure 4).

3.5.2. Interpretation

The sorted bioturbated coarse sandy silt with dispersed clasts of LSU 5 likely represents an ice-distal open-marine depositional environment with ice-rafted debris deposition affected by strong currents. These sediments also include relatively diverse assemblages of benthic foraminifera with species characteristic of the modern Antarctic outer continental shelf in water depths < 500 m (Eyles et al., 2001) and the diatoms *Paralia sulcata* and *Thalassionema nitzschioides*, indicating saline nutrient-rich possibly shallow waters and/or the proximity of the Polar Front Zone (Winter and Iwai, 2002; Bart and Iwai, 2012; Kato et al., 2020).

3.6. Lithostratigraphic Unit 6 (LSU 6)

3.6.1. Massive clast-poor to clast-rich diamict

Sediments between 313 and 344 mbsf (Cores 37R to 40R) show a gradational change in clast size and abundance and range from clast-poor massive diamictites with small pebbles at the bottom of the unit to clast-rich massive diamictites at the top (Shipboard Scientific Party, 1999). Despite the variations in clast size and abundance, matrix grain-size of the diamictites is uniform downcore and very fine grained and poorly sorted with a broad mode in the fine silt range (Figure 4).

3.6.2. Interpretation

In LSU 6, clast-poor diamictites at the bottom contain assemblages of foraminifera typical of ice-proximal glaciomarine environments with low salinity and high sedimentation rates (Eyles et al., 2001). The presence of foraminifera and variation and gradational change in clast size and abundance point to possible deposition from floating ice becoming more ice-proximal upward. Poorly preserved and broken benthic foraminifera in the clast-rich diamictites at the top of LSU 6 indicate sediment transport onto the continental shelf that involved subglacial deformation and/or debris flow activity (Eyles et al., 2001). The uniformity and very fine grain size of the diamictites with a high clay content of the matrix is indicative of deformation tills typical of glacial settings with significant meltwater at the bed that incorporate fine-grained interglacial marine sediments (e.g. Passchier et al., 2010). The uniformity and fine grain-size of the sediment matrix in this unit precludes extensive bottom current activity, which would be expected in a proglacial ice-shelf setting (Prothro et al., 2018; Smith et al., 2019).

4. COMPOSITION OF 1097 SEDIMENTS

4.1. Clast petrology

Clasts in stratified and massive diamictites between ~82 and 121 mbsf at Site 1097 are predominantly basalt with clasts of mafic plutonic and volcaniclastic lithologies present as well (Shipboard Scientific Party, 1999)(Figure 6). Andesite/rhyolite is increasing in abundance from 111 to 122 mbsf, with a minor contribution from plutonic and volcaniclastic lithologies, whereas metamorphic lithologies are absent. In gravel-rich lithologies between ~130 and 200 mbsf, plutonic rocks dominate, while metamorphic and volcaniclastic lithologies are also present. In massive and stratified diamictites between ~217 and 275 mbsf basalt and andesite/rhyolite are dominant with additional contributions from plutonic and metamorphic rocks. Clasts were not counted in the mudstones. Clasts in the diamictites between ~332 and 343 mbsf are from volcaniclastic and plutonic sources.

4.2 Trace and rare earth element ratios

The elemental ratios Gd_N/Yb_N, Eu/Eu*, Ti/Nb, Th/U and Y/Ni show variability downcore (Figure 7) and can be used to identify different types of source rocks and the effects of sorting, weathering and recycling on the sediment geochemistry (McLennan et al., 1990, 1993, Bonjour and Dabard, 1991)(Figure 8). 'N' designates chondrite-normalized values according to Bhatia (1985). The compatible element Europium is extracted from the magma through incorporation in plagioclase, and residual magmas have a negative europium anomaly and a high Eu/Eu* ratio, calculated as (Bhatia, 1985):

$$Eu/Eu^* = Eu_N /((Sm_N + Gd_N)/2)$$

Gd_N/Yb_N ratios are relatively constant downcore with lower values in stratified diamictite ~120 mbsf, the top of the mudstone at ~285 mbsf and the mudstone and stratified diamictite at ~305-335 mbsf (Figure 7). Eu/Eu* values are even more uniform with values ~0.7-0.8. Ti/Nb values show a decrease downsection, with a step-decrease at ~218 mbsf at the boundary between LSU 2 and 3. Very high Th/U values are observed in the stratified diamictite at ~117-130 mbsf and Th/U values are also elevated in the massive diamictites of LSU 3 between 218 and 284 mbsf. However, Th/U values abruptly decrease downcore at ~217-218 mbsf before increasing below ~218 mbsf. Y/Ni values are constant above ~218 mbsf, but fluctuate below that level, where maxima in Y/Ni values are found in thin stratigraphic intervals.

The low Gd_N/Yb_N ratios and relatively high Eu/Eu* values are consistent with a predominantly intermediate to mafic low-pressure magmatic rock source for the sediments, such as a young arc terrane (Figure 8A)(McLennan et al., 1990; 1993). The Ti/Nb values at Site 1097 are high and indicate a contribution from arc-volcanic terrains (Bonjour and Dabard, 1991). Ti/Nb values are generally higher in magmas derived from slab melting during subduction and relatively low in rocks developed in fore-arc basins (Figure 8B). The change in Ti/Nb ratios at ~218 mbsf (Figure 7) indicates a change in bulk sediment provenance, as this ratio is not sensitive to sediment sorting or weathering (Bonjour and Dabard, 1991).

Th vs. Th/U values are representative of active margin muds and fall between rocks originating from depleted mantle sources and continental crust (Figure 8C). An intermediate to felsic source is evident in the Y/Ni and Cr/V ratios (Figure 8D). Ni represents the general level of ferromagnesian trace elements, whereas Y serves as a proxy for Heavy Rare Earth Elements (HREE)(McLennan et al., 1993). The more abundant ferromagnesian minerals in ultra-mafic to mafic sources decrease the Y/Ni ratio, whereas the absence or paucity of ferromagnesian minerals in sediment derived from intermediate to felsic sources results in higher Y/Ni values. Although the Y/Ni ratio may also be affected by grain-size as Y is concentrated in the clay fraction (Fralick and Kronberg, 1997) there is no correlation between Y/Ni values and clay percent in our case, suggesting that the downcore changes primarily represent changes in provenance. Thus, the higher Y/Ni values below ~217 mbsf indicate a larger contribution from a felsic source than is generally observed above ~217 mbsf (Figures 7 and 8D). In addition, the Cr/V ratios are generally high in ophiolites due to the presence of chromite (McLennan et al., 1993), but the relatively low Cr/V values in 1097 sediments are consistent with an intermediate or felsic source (Figure 8D). Furthermore, both Hf vs. La/Th and Zr/Sc vs. Th/Sc biplots show values consistent with an intermediate to felsic source or acidic arc provenance (Figures 8E and 8F)(Floyd and Leveridge, 1987; McLennan et al., 1993). The lack of Zr enrichment is also indicative of a negligible effect of sediment sorting and recycling and a dominant provenance imprint on the detrital geochemistry (McLennan et al., 1993).

4.3 Provenance

The high Ti/Nb ratios in Site 1097 sediments above ~218 mbsf (LSU 1 and 2) may include a larger contribution from the Jurassic and younger arc volcanic rocks, which are most widespread

in the higher elevation regions of northwestern Palmer Land (Figures 1 and 2), than the rocks below ~218 mbsf. Granites, gabbros, basalts, andesites and rhyolites related to the Jurassic-Cretaceous accretionary complex in the region generally have a range of Ti/Nb values that are typically > 700 with gabbros on the eastern margin of George VI sound exhibiting very high Ti/Nb > 1000 and Zr values < 100 ppm (Wareham et al., 1997; McCarron & Smellie, 1998; Riley et al., 2020). Although rocks of the accretionary complex of Alexander Island with allochtonous oceanic basalts also exhibit some high Ti/Nb values (Doubleday et al., 1994), the high Y/Ni and low Cr/V ratios of the Site 1097 sediments (Figure 8D) suggest that any contribution from an ophiolite source was limited (McLennan et al., 1993). Furthermore, the fore-arc volcaniclastic rocks of the LeMay group of Alexander Island and Cenozoic alkalic basalts have Ti/Nb values < 500 (Hole, 1988, 1990, 1993 and Willan, 2003)(Figure 8B).

5. AGE MODEL

We do not adopt the diatom ranges derived from ODP Site 1095 that have been used for earlier age constraints at Site 1097 (e.g., Bart and Iwai, 2012), because of unexplained discrepancies between the magnetostratigraphy and the diatom biostratigraphy at Site 1095 that have also been highlighted elsewhere (Hillenbrand and Ehrmann, 2005; Tauxe et al., 2012; Kato et al., 2024). In addition, diachroneity in First Occurrences (FO) between deep-sea and high latitude continental shelf sites, where shelf sites are typically colonized later, was also not considered previously. Therefore, a new age model (Figure 9) is constructed for the Pliocene interval of Site 1097 using published diatom and radiolarian occurrences and zonations combined with sparse magnetostratigraphy (Shipboard Scientific Party, 1999; Iwai and Winter, 2002). For this new age model, diatom ages were derived using updated ranges in Winter and Iwai (2002), McKay et al. (2019), and Kato et al. (2024). Last appearance datums (LAD) were used where an assemblage of multiple co-occurring species provided confidence to the Last Occurrence (LO), whereas the presence of sparse fragments or single specimen occurrences were treated with caution due to potential reworking.

5.1. Diatom and radiolarian occurrences

We examine strata between 82 and 343 mbsf, where core recovery and microfossil preservation are sufficient for paleoclimatological reconstructions of the Pliocene stratigraphic record. The upper ~80 m of Site 1097 is largely barren or contains potentially reworked material, but poorly

preserved diatom and nannofossil specimens suggest a Pleistocene age (Iwai and Winter, 2002). For example, *T. fasciculata* with a range of ~4.5-0.9 Ma is present in Sample 8R-CC at ~63 mbsf. *T. torokina, T. oestrupii, T. oliverana*, and more fragments of *T. fasciculata*, are found in Samples 178-1097A-9R-CC through 11R-CC (~72-92 mbsf) and provide a Pliocene age for the interval below 72 mbsf (Shipboard Scientific Party, 1999).

Cores 1097A-12R through 19R at ~103-150 mbsf were placed in the *T. inura* Zone subzone b by Iwai and Winter (2002), which typically is assigned an age range of 4.7-4.5 Ma to 4.4 Ma (McKay et al., 2019; Kato et al., 2024)(Figure 9). However, diatoms are common in Sample 1097A-16RCC ~126 mbsf (Iwai and Winter, 2002), where *Fragilariopsis aurica* and *F. praecurta* with a LAD of 4.2 Ma (Kato et al., 2024) are found, with only one presence of *F. praecurta* above it in Sample 13R-CC ~112 mbsf, which could be reworked. Sample 1097A-16RCC ~126 mbsf also contains *T. complicata* and *T. striata* (Iwai and Winter, 2002), which have been assigned a FAD of ~4.5 Ma in the Ross Sea (McKay et al., 2019). This suggests an age between ~4.5 and 4.2 Ma for Sample 1097A-16R-CC to -13CC between ~126 and 112 mbsf, and the sediments ~112 mbsf could be even younger than 4.2 Ma if reworking is implied. The FO of *T. complicata* is found in Core 22R (~169 mbsf), but it is more common in Core 19R and upward (Shipboard Scientific party, 1999). Core sections 22R-CC to 27R-1 ~170-219 mbsf were assigned to the *T. inura* Zone subzone a by Iwai and Winter (2002) with a range of ~4.9-4.5 Ma reported at most Southern Ocean and Antarctic Sites (Kato et al., 2024). Core 34R-CC (~289 mbsf) has common diatoms, and the presence (possibly LO) of *T. oliverana v. sparsa* suggests an age of at least ~4.9 Ma (Figure 9). Isolated fragments of *T. oliverana v. sparsa* found in diamictites above this level are likely reworked.

Radiolarians in Sample 178-1097A-12R-CC (~112 mbsf) to -25R-CC (~200 mbsf) all belong to the Upsilon zone, but many are fragmented (Shipboard Scientific Party, 1999). Better preserved specimens in Cores 26R-28R (~209-228 mbsf) belong to the lower quartile of the Upsilon radiolarian zone (4.6-3.6 Ma), while Cores 33R-36R (~275-309 mbsf) belong to the Tau radiolarian zone (5.0-4.6 Ma).

5.2. Magnetostratigraphic data

Interpretation of the magnetostratigraphy above ~284 mbsf is challenging due to the low recovery and difficulties obtaining quality measurements from diamictites and other gravel-rich

lithologies (Shipboard Scientific Party, 1999). Nevertheless, the available data complement the biostratigraphic interpretations, even though the reversals fall in gaps between recovered cores (Figure 9). The mudstones between ~284 and 310 mbsf have a higher recovery, and higher quality measurements in these fine-grained lithologies provide clearly defined inclinations. Several magnetostratigraphic reversals are identified, that are expected when applying the chonostratigraphy based on the updated biostratigraphic zonations (Figure 9).

6. EARLY PLIOCENE ICE-SHEET HISTORY

Time series of glacial dynamics are not well-studied in drillcores from Antarctic continental shelves, even though ice-proximal deposits provide unique direct evidence on the paleoglaciology of an ice-sheet system that cannot be acquired from ice-distal sites (Bart et al., 2007). Coincidentally, the timing of Pliocene phases of shelf aggradation and progradation in particular, whether synchronous or not around the Antarctic margin, and how these phases relate to changes in Pliocene high-latitude climate and ice-sheet drainage systems, have been debated for many years (Cooper et al., 1991; Larter et al., 1997; Bart, 2001; Rebesco et al., 2006; Larter, 2007; O'Brien et al., 2007; Bart and Iwai, 2012; Hernández-Molina et al., 2017; Gohl et al., 2021). Sparse data collection on drillcores from the continental shelves currently limits groundtruthing of seismic interpretations and ice-sheet model validation with geological data (Halberstadt et al., 2024). While the limitations of low recovery, chronology and hiatus due to glacial erosion provide discontinuous paleo-records, ice-proximal sites have provided crucial information about long-term changes in climate and glacial dynamics of Antarctica (e.g., Bart and Iwai, 2012; Hauptvogel and Passchier, 2012; Orejola et al., 2014; Reinardy et al., 2015; Anderson et al., 2011; Tibbett et al., 2021; Marschalek et al., 2022; Klages et al., 2024).

The response of the APIS to early Pliocene phases of warming is elucidated by the sedimentary record of ODP Site 1097. The record of Site 1097 also documents the transition of the APIS from a thin ice sheet with multiple ice centers into a fully coalesced ice sheet with ice advances across the continental margin. The geometry of strata on the George VI Land continental margin off Marguerite Bay is characterized by a transition of only slightly progradational semi-horizontal stacking without the presence of a clear shelf break in Seismic Package 3, to steep clinoforms exhibiting more than 2-3 km of shelf edge progradation in Package 2 (Bart and Iwai, 2012)(Figure 3). Below we integrate the new data from Site 1097 with previously published

insights from the seismic stratigraphy (Bart et al., 2005; Bart and Iwai, 2012; Hernández-Molina et al., 2017)(Figure 3)(Table 1). We emphasize that the correlation between the seismic data and cores across the George VI Land Margin is beyond the scope of this work, and that several slightly different seismic-core correlations are used for Site 1097, as discussed by Hernández-Molina et al. (2017). Instead, our objective here is to provide a relatively narrow stratigraphic context for the new sedimentological and provenance data of Site 1097 based on previously published and broadly consistent interpretations of stratal geometries in seismic data around Marguerite Bay (Bart et al., 2005; Bart and Iwai, 2012; Hernández-Molina et al., 2017).

6.1. Early Pliocene marine ice-sheet instability ~5.2-4.5 Ma

During the progradational stacking phase, corresponding to Seismic Package 3 (Bart et al., 2005)(Figure 3), the morphology and slope of the continental margin were very different from today (Larter et al., 1997). These boundary conditions affect continental shelf and slope sedimentary processes on glaciated continental margins (Ó Cofaigh et al., 2003). A mid-shelf high may still have inhibited ice advance to the shelf break and may have blocked sediment transfer to the slope and rise (Hernández-Molina et al., 2017). Instead, sediment accumulated in the mid-to-outer shelf, where it was preserved due to ongoing subsidence (Larter et al., 1997).

Lithostratigraphic Units 6 to 3 (~344-219 mbsf) fall within Seismic Package 3 and this core interval is tied to seismic units with retrogradational and progradiational to aggradational internal geometries between reflector 3.14 and 3.9 of Bart et al. (2005)(Figure 3). The diatom assemblages in this interval of Site 1097 suggest that the bathymetry of the shelf was shallower than today (Bart and Iwai, 2012). While troughs several tens of meters deep and tens of kilometers wide are identified in Seismic Package 3, they do not appear to exhibit cross-shelf orientations and no evidence for a role of ice streams in their excavation could be found (Bart et al., 2005). Instead, erosion of the troughs in Seismic Package 3 is interpreted to have occurred through other glaciogenic processes or headward erosion in an upper slope setting, not necessarily requiring the presence of grounded ice over Site 1097. Deposition was envisioned to have taken place along a linear front (Bart et al., 2005).

6.1.1. Early Pliocene ice retreat ~5.2-4.9 Ma

We attribute the grain-size properties (Figures 4 and 5) and clast-stratified nature of the diamictite in LSU 6 (~344-313 mbsf) to deposition in a glaciomarine environment during a phase of ice expansion before ~5.2 Ma (Table 1). The upward transition from more ice-distal to ice-proximal glaciomarine deposition within LSU 6 is supported by earlier sedimentological, paleo-ecological and seismic stratigraphic interpretations (Eyles et al., 2001; Bart et al., 2005). The abrupt upward grain-size and facies change to intensely bioturbated mud with ice-rafted debris in LSU 5 (~309-303 mbsf) signifies a transition to an open-marine environment with rare icebergs followed by prolonged glacial retreat between ~5.2 and 5.0 Ma. According to our age model (Figure 9), the decrease in grain-size is accompanied by a sharp drop in sedimentation rates, which would be expected in a more ice-distal setting away from the direct input of glacial sediment.

The overlying interbedded laminated and deformed sandy muds with ice-rafted debris in LSU 4 (~296-284 mbsf) are interpreted as evidence of more intense iceberg rafting and meltwater plumes indicating a greater proximity of the ice margin between ~5.0 and 4.8 Ma. The depositional environment was still shallow (Bart and Iwai, 2012) which would have been conducive to glacial advance. However, the fine matrix grain-sizes in LSU 4 and low sedimentation rates indicate that sediment delivery from a nearby major ice outlet was unlikely.

LSUs 6 to 4 have low pebble count, including mafic plutonic, granite/granodiorite and volcaniclastic lithologies with matrix geochemical results indicating felsic-intermediate (high Y/Ni) and fore-arc sedimentary (low Ti/Nb) sources. In igneous rocks, Gd_N/Yb_N ratios are elevated in tonalites and sodic granodiorites (McLennan et al., 1990). The slightly higher Gd_N/Yb_N in LSUs 4 and 5 (Figure 7) are consistent with enhanced sediment delivery from plutonic, volcanic and sedimentary rocks from local glaciers on the northern part of Alexander Island, Adelaide Island or the coastal sections of Marguerite Bay (Figure 2).

The generally low pebble abundance, its composition and the matrix provenance for LSU 6 through 4 point to local sediment sources, interpreted as sediment delivery from a local ice cap or piedmont glacier between ~5.2 and 4.8 Ma. The shifts in detrital provenance as interpreted from the trace element and REE ratios likely represent changes in the local sources of ice-rafted debris and meltwater plumites (Figure 7).

6.1.2. Ice advance and retreat ~4.8-4.5 Ma

The massive clast-rich diamictites with a very poorly sorted matrix in the lower part of LSU 3 (~276-265 mbsf) were deposited in an ice-contact environment, either through deposition from floating ice or subglacially ~4.8 Ma. LSU 3 is defined within a unit showing a decrease in progradation within the upper part of Seismic Package 3 (Bart et al., 2005)(Figure 3). Hernández-Molina et al. (2017) trace the base of glacial margin sequences (BGMS) to a change from glaciomarine to subglacial deposition, which at Site 1097 occurs at the base of LSU 3.

The high Th/U values in the massive diamictites of LSU 3 between 218 and 284 mbsf coincide with high abundances of andesite/rhyolite clasts, whereas granite/ granodiorite, volcaniclastic and metamorphic clasts are also common (Figure 6). The dominance of andesitic-rhyolitic, granite/granodiorite and metamorphic rocks and the more felsic geochemical signature (Th/U ratios) of the diamictite matrix would suggest a contribution from northwestern Palmer Land (Davies, 1984; Leat and Scarrow, 1994). However, this interval also has relatively low Ti/Nb ratios and high Y/Ni ratios, which could point to a larger sedimentary and/or volcaniclastic contribution to the matrix than to the rock clast assemblage. A possible explanation is preferential abrasion of more friable sediment clasts during glacial transport. The low Ti/Nb ratios of the sediment matrix may be indicative of a contribution from eroded fore-arc sediments in eastern Alexander Island or the mid-shelf high (Figure 3A). In summary: the clast assemblages and geochemical matrix provenance point to sources in northwestern Palmer Land and eastern Alexander Island indicating that separate ice centers began to coalesce into an ice sheet with an outflow across Marguerite Bay (Table 1).

A reflector tied to ~250 mbsf within the interval of washed gravel at Site 1097 is interpreted as a horizon marking only minor glacial retreat (Bart et al., 2005). In contrast, the boulder diamictites at the top of LSU 3 at ~227-219 mbsf in Cores 28-27R indicate calving of icebergs from marine ice sheets ~4.6-4.5 Ma. The presence of calcareous nannofossils of the genus *Dictyococcites* suggests that the deposition of the cobble-boulder diamictite took place under the influence of warmer water masses (Iwai et al., 2001). Furthermore, foraminiferal Mg/Ca temperature data from DSDP Site 590 show that peak warming in the South Pacific was achieved during this time (Karas et al., 2011). We argue that the increase in subsurface water mass temperature resulted in marine ice-sheet instability. Unfortunately, poor recovery of LSU 3 does not allow for a reconstruction of varying sedimentary environments for the entire sequence.

6.2. Transitional Phase ~4.5-4.3 Ma

At Site 1097 we identified a lithological contact in Core 27R between a massive cobble-boulder diamictite (top of LSU 3) and interstratified sediments (base of LSU 2). The latter contains bioturbation in isolated thin beds and benthic foraminifera that include well-preserved specimens typically found on the Antarctic continental shelf (Eyles et al., 2001). The disconformity in Core 27R at ~219 mbsf that separates LSU 3 from LSU 2 is also apparent in the detrital provenance data (Figure 7). Diatomaceous laminae and reworked diatoms in LSU 2 of Site 1097 provide evidence of intermittent deposition in open-marine conditions on a deep continental shelf (Shipboard Scientific Party, 1999)(Bart and Iwai, 2012).

LSU 2 (~219-179 mbsf) consists of interstratified and deformed sediments (Figure 4) and is set within the section that spans the uppermost part of Seismic Package 3 and the lowermost part of Seismic Package 2 (Figure 3A). In along-trough seismic lines the architecture of the strata at the Seismic Package 3/Package 2 transition does not show evidence of a clear shelf break and only minimal progradation (Bart et al., 2005; Bart and Iwai, 2012)(Figure 3A). Numerous seismic reflectors displaying angular unconformities of small channels with scour- and-fill geometries intersect Site 1097 at the level of LSU 2 (Bart et al., 2005, 2007). Bart et al. (2005) identified possible trough remnants through contour mapping of seismic reflectors in the upper part of Seismic Package 3, but determined that their origin was ambiguous. Cross-trough seismic data show that the sediments are thicker where they are draped within a trough to the southwest of Site 1097, and thinner at 1097, which is situated on the eastern flank of the trough (Figure 3B). Hernández-Molina et al. (2017) regard the Seismic Package 3/Package 2 boundary section (their Seismic Unit 4) as a transitional unit, with an onset of trough formation (Figure 3B).

6.2.1 Sedimentary processes and glacial regime

The interstratified character of the sediments in LSU 2 and the extensive soft-sediment deformation are indicative of rapidly accumulating sediments and syn-sedimentary gravity flows. The geometry and sedimentological characteristics of the sediments in LSU 2 are consistent with an origin as multiple overlapping ice-proximal or ice-contact fans and glacigenic debris flows during glacials and hemipelagic sedimentation during interglacials. Our age model of Site 1097 suggests that sedimentation rates associated with the deposition of these interstratified sediments were extremely high, and the high pore-water pressures in these rapidly accumulated

unconsolidated sediments could have made them prone to syn-sedimentary deformation and gravity flow. The interstratified nature of the deposits and the reflectors identified in seismic data delineate multiple phases of glaciogenic deposition with gravity flows during phases of ice advance, and intermittent meltwater plume and pelagic sedimentation during phases of ice retreat. The low relief of the paleotroughs, the minimal progradation and the meltwater dominated facies in LSU 2 do not resemble modern or Pleistocene shelf-slope environments of retreating ice streams in Antarctica (e.g., Ó Cofaigh et al., 2003; 2005; Passchier et al., 2003) and are instead known from glaciomarine settings or low-gradient upper continental slope deposition with considerable meltwater influence in the Northern Hemisphere (Gustavson and Bootroyd, 1987; Powell and Molnia, 1989; Lønne, 1995; Ó Cofaigh et al., 2003).

The accumulation of LSU 2 is dated to between ~4.5 and 4.4 Ma and marks the onset of a dynamic ice-sheet system periodically grounded on the George VI Land continental shelf with characteristics of a warmer glacial regime than currently encountered in Antarctica. Deposition of ice-contact fans is generally associated with a stillstand in ice retreat, but their accumulated thickness typically also requires episodes of extreme meltwater discharge and high sedimentation rates (Batchelor and Dowdeswell, 2015), with high glacial erosion rates and episodic fast flow (Pritchard and Vaughan, 2007). These interpretations point to the development of a high accumulation- fast through-put glacial regime (Vaughan, 2006).

6.2.2 Sediment provenance and ice development

Plutonic, metamorphic and volcaniclastic lithologies are dominant in the well-sorted sediments of LSU 2 (Figure 6). $^{39}Ar/^{40}Ar$ ages of 75–173 Ma were obtained for volcanic clasts in stratified diamictite at 178-1097A-27-1, 35–58 cm at the base of LSU 2 (218 mbsf)(DiVincenzo et al., 2002). Although it was noted that the glassy material generally was heavily altered, measurements on 5 samples of 10 grains each yielded average ages of 118-142 Ma, and a milligram sized fraction an age of 122 Ma. Volcaniclastic rocks of this age are widespread in the Fleming Glacier catchment of northwestern Palmer Land and on Adelaide Island (Leat et al., 2009), where the presence of mafic plutonic and metamorphic basement rocks explains the elevated Ti/Nb ratios (Figure 2). Although similar volcaniclastic rocks with high Ti/Nb ratios are also found in central Alexander Island, the uplands preserve late Miocene subglacially erupted

volcanic rocks (Smellie et al., 2009), making extensive glacial erosion of central Alexander Island in the Pliocene or thereafter unlikely.

6.3. Onset of ice advances to the shelf break by ~4.3 Ma

LSU 1 falls within Seismic Package 2 (Figure 3) with sediments analyzed in Cores 19R through 10R above ~150 mbsf. The sediments consist of massive and stratified diamictites with uniform matrix grain-size distributions (Figures 3 and 4), similar to modern or recent Antarctic sediments that were deposited by ice streams extending across the continental shelf (Ó Cofaigh et al., 2005; Prothro et al., 2018). Seismic Package 2 is characterized with a transition to prograding clinoforms seaward of the Marguerite Trough (Larter et al., 1997; Bart et al., 2005; Bart and Iwai, 2012). Interpretations of Seismic Package 2 suggest that during deposition ice advances led to progradation of the George VI Land continental shelf (Bart and Iwai, 2012). Over multiple glacial cycles ice streams carved cross-shelf flow paths northward through Marguerite Bay and delivered sediment to the continental slope (Figure 3A). According to Eyles et al. (2001) a change to more persistent subglacial deposition is evident above ~150-180 mbsf in the sediments at Site 1097, which is also confirmed by our data interpretations of LSU 1. Interpretations of diatom taxa at Site 1097 above ~150 mbsf indicate a deep shelf environment for retreat phases (Bart and Iwai, 2012).

Especially within the diamictites in LSU 1, clast counts show a high abundance of andesite/rhyolite and basalt clasts (Figure 6). Because Pliocene erosion of the central uplands of Alexander Island is unlikely, as mentioned above, LSU 1 sediments are probably sourced primarily from northwestern Palmer Land along Fleming Glacier, and the margin of the George VI Sound (Davies, 1984; Smith, 1987) (McCarron and Smellie, 1998; Riley et al., 2023)(Figure 2). Basalt pebble counts increase upward within LSU 1 with a maximum in the massive diamictite at the top above ~122 mbsf, where Ti/Nb ratios are also high. In northwest Palmer Land basalts are prevalent near the mouth and along the eastern margin of George VI Sound, between Cape Jeremy and Fleming Glacier (Leat and Scarrow, 1994; Leat et al., 2009)(Figure 2).

In a thin section of LSU 1, very high Th/U values in a stratified diamictite at ~117-130 mbsf (Figure 7) indicate a strong felsic contribution or delivery of weathered sediment (Figure 8). The high Th/U values can be explained by a period of enhanced erosion in the George VI Sound and Marguerite Bay into sediments of the Fossil Bluffs Group, east of the LeMay Fault (Figure 2).

Within this stratified diamictite, a bed with a large proportion of andesitic/rhyolitic clasts is present at 121-123 mbsf and > 0.5 cm clast abundance is counted as > 35 clasts per meter of core depth. This event may signal extensive calving of the marine ice-sheet system occupying the Marguerite Bay and Trough with a large proportion of icebergs dumping debris. The variability in facies, including diatom laminae, grain-size and provenance ~130-120 mbsf result from an unstable marine ice sheet ~4.2 Ma.

Applying our lithostratigraphic and provenance interpretations within an updated age model, we conclude that progradation related to the advanced erosion of a cross-shelf trough, commenced by ~4.3 Ma. After ~4.2 Ma the APIS had episodes of extensive growth, but poor age control and low core recovery at Site 1097 preclude any insights on the precise timing. Massive diamictites recovered between ~82 and 113 mbsf with basalts originating from the mouth of the George VI Sound, suggest a dominance of ice flow through the George VI Sound conduit towards the continental shelf edge between ~4.2 and 0.9 Ma. Hernández-Molina et al. (2017) observed that the main trough was initially located to the southwest of Site 1097 and interpreted the internal seismic geometry of Package 2 as an eastward migration of the paleotrough to the current position of the Marguerite Trough (Figure 3B). The eastward migration of the trough is consistent with our provenance record of a growing importance of the Marguerite Ice Stream conduit in APIS drainage during the early-mid Pliocene, in addition to ice flow through the Fleming Glacier conduit. The provenance of the massive diamictites between ~82 and 113 mbsf show that ice flow became channeled by the tectonic structure of George VI Sound, and confined ice flow contributed to the incision of the George VI Sound glacial trough. This reconstruction resembles ice flow during the last glacial maximum (LGM) when the George VI and Wordie catchments converged into the Marguerite Ice Stream, while the APIS inundated the topography of Palmer Land (Ó Cofaigh et al., 2005; Golledge et al., 2014).

Ice sheet models show that under modern full glacial conditions ice flow from the central APIS is channeled through the Fleming Glacier conduit into Marguerite Bay, where it merges with ice flowing out of George VI Sound into the Marguerite Trough Ice Stream (Golledge et al., 2013, Golledge, 2014). Within the Marguerite Trough Ice Stream system, the mouth of George VI Sound experiences the highest erosivity during modern full glacial conditions and reaches a maximum erosivity during deglaciation (Figure 2). Secondary locations of high erosivity are

found to the southeast of Marguerite Bay at the mouth of the modern Fleming Glacier conduit and on the inner shelf in Marguerite Bay. In the ice sheet model, the northerly summits of Alexander Island are exposed under full glacial conditions, while the central part is covered by a thin local ice dome. Ice flow out of the APIS ice divide largely flows around the topography of Alexander Island and Adelaide Island. Subglacial erosion potential is the greatest below fast-moving segments of the outlets of the APIS (Golledge, 2014)(Figure 2). The provenance signature of the Site 1097 sediments in LSU 1 supports a similar glacial configuration as predicted by the ice-sheet model of Golledge (2014).

7. ICE SHEET RESPONSE TO CLIMATE VARIABILITY

For the 5.0-4.5 Ma early Pliocene time window Tierney et al. (2025) reconstruct Southern Hemisphere polar amplification of warming of 1.9, resulting in average high-latitude surface temperatures that were ~9.1 °C warmer than pre-industrial, calling into question the stability of ice shelves on the Antarctic Peninsula (Cook et al., 2005). During this time biogenic opal contents in the sediments offshore in the Bellingshausen Sea were very high and interpreted as evidence of higher paleoproductivity, a warmer ocean surface and reduced sea ice (Hillenbrand and Ehrmann, 2005). Indeed, during the early Pliocene warm period the APIS margin experienced prolonged retreat ~5.2-4.8 Ma, which is evident in the deposition of mudstones in LSUs 4 and 5 at Site 1097 on the George VI Land continental shelf (Figure 5). Correlative continental rise strata to Site 1097 were deposited with along-slope processes dominating over down-slope processes and show development of mounded drifts in response to increases in bottom water circulation (Uenzelmann-Neben, 2006; Hernández-Molina et al., 2017, their SU 5). Furthermore, Lamy et al. (2023) determined that around 5.1-4.9 Ma (Plio3) the Antarctic Circumpolar Current had above modern strength. These correlative observations support a connection between a stronger ACC and ice-sheet retreat hypothesized to involve the effects of enhanced southward advection and upwelling of Circumpolar Deep Water (CDW) with southward-shifted oceanic fronts (Lamy et al., 2023).

APIS ice advances at ~4.8 and ~4.6 Ma at Site 1097 coincides with a weakened ACC in the Southern Ocean (Lamy et al., 2023) and appear to be synchronous with ice advances in the Ross Sea reconstructed in AND-1B (Naish et al., 2009). Although poor recovery does not allow observations for the APIS between these glacial advances, Bart et al. (2005) based on seismic

765 data indicated a minor retreat tied to ~ 4.7 Ma in our age model of Site 1097, which also
766 coincides with a minor increase of the ACC (Lamy et al., 2023).

767 Antarctic Intermediate Water and South Pacific subsurface temperatures reached a maximum
768 ~4.6 Ma and stayed high until ~4.3 Ma (Karas et al., 2011). Although hiatus are present in the
769 early Pliocene of AND-1B, diatomite sequences dated to ~4.6-4.5 and ~4.4-4.3 Ma indicate
770 periods of early Pliocene ice retreat in the Ross Sea (Naish et al., 2009). These diatomites
771 produced a "subantarctic" diatom flora, currently found only north of the Polar Front Zone, and
772 organic biomarker evidence of SST up to ~5 °C warmer than present (McKay et al., 2012).
773 Furthermore, ungrounding and retreat of the Thwaites Glacier drainage system of the West
774 Antarctic Ice Sheet is recorded ~4.6-4.4 Ma in a sediment drift in the Amundsen Sea (Passchier
775 et al., 2025). At Site 1097 a cobble-boulder diamictite with a nannofossil flora points to ocean
776 forcing of a marine ice-sheet collapse ~4.6-4.5 Ma and it is followed ~4.5 Ma by major ice
777 retreat. However, the ACC intensity dropped and stayed weak ~4.6-4.3 Ma, despite elevated
778 SSTs until ramping up again to another phase of above modern strength ~3.8 (Lamy et al., 2023).

779 Following ice shelf collapse and retreat, the sedimentology of LSU 2 at Site 1097 is interpreted
780 as sediment delivery from a maritime "subpolar" front producing slope fans composed of
781 deformed glaciomarine and meltwater plume deposits ~4.5-4.4 Ma with bioturbated
782 diatomaceous sediments in this unit representing interglacial retreat. The ~4.5-4.4 Ma APIS
783 advances to the mid-outer shelf and sharp retreat seem to contrast with the West Antarctic Ice
784 Sheet records from the Ross and Amundsen Seas. However, for high elevation terrestrial ice
785 sheets, such as the APIS, the positive effect of warming on snow accumulation could have
786 dominated the ice-sheet mass balance. Deposition of LSU 2 at Site 1097 between ~4.5 and 4.4
787 Ma occurred under a different glacial regime than the last glacial maximum and deglaciation.

788 The development of ice lobes and meltwater fans with diatom-rich interbeds is consistent with
789 the establishment of a dynamic high accumulation – large through-put glacial system. Notably,
790 the interpretations of core data from Site 1097 are consistent with the Pliocene ice-sheet
791 modeling of Halberstadt et al. (2024). In the ice-sheet model terrestrial ice sheets with marine
792 outlets stay intact after ~4.5 Ma because accumulation outweighs marine ice-sheet mass loss
793 even when marine ice-sheet grounding lines are retreating (Halberstadt et al., 2024). This model
794 does not include variable ocean forcing and excludes the earliest Pliocene before 4.5 Ma, when

paleorecords indicate more extensive high-latitude warming and episodes with a stronger ACC than present (Tierney et al., 2025; Lamy et al., 2023). The model does incorporate marine-ice cliff instability, and even though the APIS stays intact, marine ice sheets disintegrate under maximum interglacial early Pliocene greenhouse and insolation forcing (Halberstadt et al., 2024).

LSU 1 shows that major ice expansion of the APIS with glacial erosion on the continental shelf and progradation of the George VI Land slope likely commenced by ~4.3 Ma. In ODP Site 1103 farther northwest on the Antarctic Peninsula continental shelf the stratigraphy is poorly recovered and based on available biostratigraphic data a seismic unconformity there is interpreted as an hiatus spanning the early-mid Pliocene (Eyles et al., 2001). Farther to the southwest, AND-1B in the Ross Sea, regarded as a West Antarctic Ice Sheet record, also exhibits an hiatus spanning ~4.3-3.6 Ma (Naish et al., 2009). These hiatus could represent amalgamated surfaces of glacial erosion. In addition, numerical modeling has shown evidence of ice-sheet instability in the high insolation interglacial ~4.2 Ma (Golledge et al., 2017). Although there is no evidence for prolonged retreat at ~4.2 Ma at Site 1097 the stratified diamictites with a distinct provenance signature represent a response of the George VI land ice-sheet system to warming driven by high-latitude insolation. Lack of recovery and age control at Site 1097 do not allow for ground-truthing of the paleoglaciology for the interval younger than ~4.2 Ma.

8. CONCLUSIONS

Site 1097 comprises a unique early Pliocene marine sediment archive on the Pacific continental shelf of West Antarctica. The new sedimentological and detrital provenance insights gained from Site 1097 show evidence of glaciomarine depositional environments throughout, although with distinct changes in glacial regime and ice-sheet extent relative to the outer continental shelf (Table 1).

- Open marine environments with sparse icebergs characterize the 5.2-4.8 Ma period, indicating a time when ice was largely absent from the George VI margin, with sediment delivery from local ice caps
- Episodes of ice growth are reconstructed for~4.8 and 4.6 Ma during which outlets from local ice caps on Palmer Land and Alexander Island periodically coalesced into a marine ice sheet.

- A change in provenance of 1097 sediments dated to ~4.5 Ma indicates a transition to dominant ice flow and sediment delivery from Palmer Land, and the growth of a large APIS.
- Accumulation-driven ice advances between ~4.5 and 4.3 Ma appear to represent a different "warmer" glacial regime on the Antarctic Peninsula with ice sheets that lacked large ice shelves and fed glaciogenic sedimentation on a low-grade slope.
- Cooling from ~4.3 Ma resulted in the establishment of an ice stream that expanded and prograded the shelf edge. For this "colder" glacial regime the record from Site 1097 confirms that the APIS ice streams in the Marguerite Trough remained sensitive to insolation changes ~4.2 Ma, but that it did not result in prolonged phases of ice retreat over multiple glacial-interglacial cycles.

Early Pliocene ~5.2-4.8 Ma open marine conditions in Marguerite Bay coincided with a strengthening of the ACC (Lamy et al., 2023). Around ~4.6-4.3 Ma, periods of open marine conditions and sea surface temperatures appear to be synchronous across the Pacific margin indicating a regional ocean forcing of marine ice sheets even though the ACC weakened. However, in the warm early Pliocene terrestrial high accumulation ice sheets such as the APIS responded differently from fully marine ice-sheet drainage basins with ice advances and high sedimentation rates of meltwater-dominated sediments on the outer continental shelf.

ACKNOWLEDGEMENTS

This project used samples provided by the International Ocean Discovery Program (IODP). U.S. Gulf Coast Repository staff is thanked for providing images of sample halves and for sampling the cores. Funding was provided by the National Science Foundation Award # 2114839 to Sandra Passchier.

DATA AVAILABILITY

Data will be made accessible upon publication of the manuscript at https://www.usap-dc.org/.

AUTHOR CONTRIBUTIONS: CRediT

Sandra Passchier: Conceptualization, Data curation, Formal analysis, Funding acquisition, Investigation, Methodology, Project administration, Supervision, Visualization, Writing –

original draft, Writing – review and editing

Ridley Joseph: Formal analysis, Investigation, Writing – original draft, Writing – review and editing

Monika Ghimire: Investigation, Writing – review and editing

Xiaona Li: Methodology, Investigation

REFERENCES

Anderson, J.B. et al., 2011. Progressive Cenozoic cooling and the demise of Antarctica's last refugium. Proceedings of the National Academy of Sciences, 108(28): 11356-11360.

Bhatia, M.R., 1985. Rare earth element geochemistry of Australian Paleozoic graywackes and mudrocks: provenance and tectonic control. Sedimentary geology, 45, (1-2): 97-113.

Bart, P., 2001. Did the Antarctic ice sheets expand during the early Pliocene? Geology, 29(1): 67-70.

Bart, P. et al., 2007. Are Antarctic Peninsula Ice Sheet grounding events manifest in sedimentary cycles on the adjacent continental rise? Marine Geology, 236(1-2): 1-13.

Bart, P.J., Egan, D., Warny, S.A., 2005. Direct constraints on Antarctic Peninsula Ice Sheet grounding events between 5.12 and 7.94 Ma. Journal of Geophysical Research: Earth Surface, 110(F4).

Bart, P.J., Iwai, M., 2012. The overdeepening hypothesis: How erosional modification of the marine-scape during the early Pliocene altered glacial dynamics on the Antarctic Peninsula's Pacific margin. Palaeogeography, Palaeoclimatology, Palaeoecology, 335: 42-51.

Batchelor, C., Dowdeswell, J., 2015. Ice-sheet grounding-zone wedges (GZWs) on high-latitude continental margins. Marine Geology, 363: 65-92.

Bonjour, J.-L., Dabard, M.-P., 1991. Ti/Nb ratios of clastic terrigenous sediments used as an indicator of provenance. Chemical Geology, 91(3): 257-267.

Burgard, C. et al., 2025. Ocean warming threatens the viability of 60% of Antarctic ice shelves. Nature, 647(8088): 102-108.

879 Burton-Johnson, A., Riley, T., 2015. Autochthonous v. accreted terrane development of
880 continental margins: a revised in situ tectonic history of the Antarctic Peninsula. Journal of the
881 Geological Society, 172(6): 822-835.

882 Clark, P.U. et al., 2025. Global mean sea level over the past 4.5 million years. Science,
883 390(6770): eadv8389.

884 Cofaigh, C.Ó. et al., 2005. Flow dynamics and till genesis associated with a marine-based
885 Antarctic palaeo-ice stream. Quaternary Science Reviews, 24(5-6): 709-740.

886 Cofaigh, C.Ó., Taylor, J., Dowdeswell, J.A., Pudsey, C.J., 2003. Palaeo-ice streams, trough
887 mouth fans and high-latitude continental slope sedimentation. Boreas, 32(1): 37-55.

888 Constantino, R.R., Tinto, K.J., Bell, R.E., Porter, D.F., Jordan, T.A., 2020. Seafloor depth of
889 George VI Sound, Antarctic Peninsula, from inversion of aerogravity data. Geophysical Research
890 Letters, 47(21): e2020GL088654.

891 Cook, A.J., Fox, A.J., Vaughan, D.G., Ferrigno, J.G., 2005. Retreating glacier fronts on the
892 Antarctic Peninsula over the past half-century. Science, 308(5721): 541-544.

893 Cooper, A.K. et al., 1991. Cenozoic prograding sequences of the Antarctic continental margin: a
894 record of glacio-eustatic and tectonic events. Marine Geology, 102(1-4): 175-213.

895 Cox, S.C. et al., 2023. A continent-wide detailed geological map dataset of Antarctica. Scientific
896 Data, 10(1): 250.

897 Crame, J.A., Howlett, P.J., 1988. Late Jurassic and Early Cretaceous biostratigraphy of the Fossil
898 Bluff Formation, Alexander Islands. British Antarctic Survey Bulletin, 78: 1-35.

899 Davies, B.J. et al., 2017. Ice-dammed lateral lake and epishelf lake insights into Holocene
900 dynamics of Marguerite trough ice stream and George VI ice shelf, Alexander island, Antarctic
901 peninsula. Quaternary Science Reviews, 177: 189-219.

902 Davies, B.J., Hambrey, M.J., Smellie, J.L., Carrivick, J.L., Glasser, N.F., 2012. Antarctic
903 Peninsula ice sheet evolution during the Cenozoic Era. Quaternary Science Reviews, 31: 30-66.

904 Davies, T., 1984. The geology of part of northern Palmer Land, 103. British Antarctic Survey.

905 Davison, B.J. et al., 2023. Annual mass budget of Antarctic ice shelves from 1997 to 2021.
906 Science Advances, 9(41): eadi0186.

907 Di Vincenzo, G., Caburlotto, A., and Camerlenghi, A., 2001. 40Ar-39Ar investigation of
908 volcanic clasts in glaciogenic sediments at Sites 1097 and 1103 (ODP Leg 178, Antarctic
909 Peninsula). In Barker, P.F., Camerlenghi, A., Acton, G.D., and Ramsay, A.T.S. (Eds.), Proc. ODP,
910 Sci. Results, 178: College Station, TX (Ocean Drilling Program), 1–26.
911 doi:10.2973/odp.proc.sr.178.232.2001

912 Dorschel, B., Hehemann, L., Viquerat, S., Warnke, F., Dreutter, S., Schulze Tenberge, Y.,
913 Accettella, D., An, L., Barrios, F., Bazhenova, E., Black, J., Bohoyo, F., Davey, C., De Santis, L.,
914 Escutia Dotti, C., Fremand, A. C., Fretwell, P. T., Gales, J. A., Gao, J., Gasperini, L., Greenbaum,
915 J. S., Jencks, J. H., Hogan, K., Hong, J. K., Jakobsson, M., Jensen, L., Kool, J., Larin, S., Larter,
916 R. D., Leitchenkov, G., Loubrieu, B., Mackay, K., Mayer, L., Millan, R., Morlighem, M.,
917 Navidad, F., Nitsche, F. O., Nogi, Y., Pertuisot, C., Post, A. L., Pritchard, H. D., Purser, A.,
918 Rebesco, M., Rignot, E., Roberts, J. L., Rovere, M., Ryzhov, I., Sauli, C., Schmitt, T., Silvano,
919 A., Smith, J., Snaith, H., Tate, A. J., Tinto, K. J., Vandenbossche, P., Weatherall, P., Wintersteller,
920 P., Yang, C., Zhang, T., and Arndt, J. E., 2022, The International Bathymetric Chart of the
921 Southern Ocean Version 2, Scientific Data, 9, 275, https://doi.org/10.1038/s41597-022-01366-7.

922 Doubleday, P., Leat, P., Alabaster, T., Nell, P., Tranter, T., 1994. Allochthonous oceanic basalts
923 within the Mesozoic accretionary complex of Alexander Island, Antarctica: remnants of proto-
924 Pacific oceanic crust. Journal of the Geological Society, 151(1): 65-78.

925 Doubleday, P., Storey, B., 1998. Deformation history of a Mesozoic forearc basin sequence on
926 Alexander Island, Antarctic Peninsula. Journal of South American Earth Sciences, 11(1): 1-21.

927 Evans, J., Pudsey, C., 2002. Sedimentation associated with Antarctic Peninsula ice shelves:
928 implications for palaeoenvironmental reconstructions of glacimarine sediments. Journal of the
929 Geological Society, 159(3): 233-237.

930 Eyles, N., Daniels, J., Osterman, L.E., Januszczak, N., 2001. Ocean Drilling Program Leg 178
931 (Antarctic Peninsula): sedimentology of glacially influenced continental margin topsets and
932 foresets. Marine Geology, 178(1-4): 135-156.

Fedorov, A.V. et al., 2013. Patterns and mechanisms of early Pliocene warmth. nature, 496(7443): 43-49.

Floyd, P., Leveridge, B., 1987. Tectonic environment of the Devonian Gramscatho basin, south Cornwall: framework mode and geochemical evidence from turbiditic sandstones. Journal of the Geological Society, 144(4): 531-542.

Fox-Kemper, B. et al., 2021. Climate change 2021: The physical science basis. Contribution of working group I to the sixth assessment report of the intergovernmental panel on climate change. Cambridge Univ. Press.

Fralick, P., Kronberg, B., 1997. Geochemical discrimination of clastic sedimentary rock sources. Sedimentary Geology, 113(1-2): 111-124.

Friedl, P., Seehaus, T.C., Wendt, A., Braun, M.H., Höppner, K., 2018. Recent dynamic changes on Fleming glacier after the disintegration of Wordie ice shelf, Antarctic peninsula. The Cryosphere, 12(4): 1347-1365.

Gohl, K. et al., 2021. Evidence for a highly dynamic West Antarctic ice sheet during the Pliocene. Geophysical Research Letters, 48(14): e2021GL093103.

Golledge, N.R., 2014. Selective erosion beneath the Antarctic Peninsula Ice Sheet during LGM retreat. Antarctic Science, 26(6): 698-707.

Golledge, N.R. et al., 2013. Glaciology and geological signature of the Last Glacial Maximum Antarctic ice sheet. Quaternary Science Reviews, 78: 225-247.

Golledge, N.R. et al., 2017. Antarctic climate and ice-sheet configuration during the early Pliocene interglacial at 4.23 Ma. Climate of the Past, 13(7): 959-975.

Gustavson, T.C., Boothroyd, J.C., 1987. A depositional model for outwash, sediment sources, and hydrologic characteristics, Malaspina Glacier, Alaska: A modern analog of the southeastern margin of the Laurentide Ice Sheet. Geological Society of America Bulletin, 99(2): 187-200.

Halberstadt, A.R.W., Gasson, E., Pollard, D., Marschalek, J., DeConto, R.M., 2024. Geologically constrained 2-million-year-long simulations of Antarctic Ice Sheet retreat and expansion through the Pliocene. Nature Communications, 15(1): 7014.

960 Hauptvogel, D.W., Passchier, S., 2012. Early–Middle Miocene (17–14 Ma) Antarctic ice
961 dynamics reconstructed from the heavy mineral provenance in the AND-2A drill core, Ross Sea,
962 Antarctica. Global and Planetary Change, 82: 38-50.

963 Hernández-Molina, F.J., Larter, R.D., Maldonado, A., 2017. Neogene to Quaternary stratigraphic
964 evolution of the Antarctic Peninsula, Pacific Margin offshore of Adelaide Island: Transitions
965 from a non-glacial, through glacially-influenced to a fully glacial state. Global and Planetary
966 Change, 156: 80-111.

967 Hillenbrand, C.-D. et al., 2017. West Antarctic Ice Sheet retreat driven by Holocene warm water
968 incursions. Nature, 547(7661): 43-48.

969 Hole, M., 1988. Post-subduction alkaline volcanism along the Antarctic Peninsula. Journal of the
970 Geological Society, 145(6): 985-998.

971 Hole, M., 1990. Geochemical evolution of Pliocene-Recent post-subduction alkalic basalts from
972 Seal Nunataks, Antarctic Peninsula. Journal of Volcanology and Geothermal Research, 40(2):
973 149-167.

974 Hole, M., Kempton, P., Millar, I., 1993. Trace-element and isotopic characteristics of small-
975 degree melts of the asthenosphere: Evidence from the alkalic basalts of the Antarctic Peninsula.
976 Chemical Geology, 109(1-4): 51-68.

977 Holt, T.O., Glasser, N.F., Quincey, D.J., Siegfried, M., 2013. Speedup and fracturing of George
978 VI ice shelf, Antarctic peninsula. The Cryosphere, 7(3): 797-816.

979 Iwai, M., Kameo, K., and Miyake, N., 2001. Calcareous nannofossils, pollen, and spores from
980 Leg 178 Sites 1095, 1097, 1100, and 1103, western Antarctic Peninsula: age constraints and
981 environmental implications. In Barker, P.F., Camerlenghi, A., Acton, G.D., and Ramsay, A.T.S.
982 (Eds.), Proc. ODP, Sci. Results, 178: College Station, TX (Ocean Drilling Program), 1–22.
983 doi:10.2973/odp.proc.sr.178.227.2001

984 Iwai, M., and Winter, D., 2002. Data report: taxonomic notes of Neogene diatoms from the
985 western Antarctic peninsula: Ocean Drilling Program Leg 178. In Barker, P.F., Camerlenghi, A.,
986 Acton, G.D., and Ramsay, A.T.S. (Eds.), Proc. ODP, Sci. Results, 178: College Station, TX
987 (Ocean Drilling Program), 1–57. doi:10.2973/odp.proc.sr.178.239.2002

Jamieson, S.S. et al., 2012. Ice-stream stability on a reverse bed slope. Nature Geoscience, 5(11): 799-802.

Jenkins, A., Jacobs, S., 2008. Circulation and melting beneath George VI ice shelf, Antarctica. Journal of Geophysical Research: Oceans, 113(C4).

Johnson, J.S., Smellie, J.L., Nelson, A.E., Stuart, F.M., 2009. History of the Antarctic Peninsula Ice Sheet since the early Pliocene—evidence from cosmogenic dating of Pliocene lavas on James Ross Island, Antarctica. Global and Planetary Change, 69(4): 205-213.

Karas, C., Nürnberg, D., Tiedemann, R., Garbe-Schönberg, D., 2011. Pliocene climate change of the Southwest Pacific and the impact of ocean gateways. Earth and Planetary Science Letters, 301(1-2): 117-124.

Kato, Y., 2020. Diatom-based reconstruction of the Subantarctic Front migrations during the late Miocene and Pliocene. Marine Micropaleontology, 160: 101908.

Kato, Y., Hernández-Almeida, I., Pérez, L.F., 2024. Diatom and radiolarian biostratigraphy in the Pliocene sequence of ODP Site 697 (Jane Basin, Atlantic sector of the Southern Ocean). Journal of Micropalaeontology, 43(1): 93-119.

Kennedy and Anderson, 1989.

Klages, J.P. et al., 2024. Ice sheet–free West Antarctica during peak early Oligocene glaciation. Science, 385(6706): 322-327.

Lamy, F. et al., 2024. Five million years of Antarctic Circumpolar Current strength variability. Nature, 627(8005): 789-796.

Larter, R., Rebesco, M., Vanneste, L., Gamboa, L., Barker, P., 1997. Cenozoic tectonic, sedimentary and glacial history of the continental shelf west of Graham Land, Antarctic Peninsula. Geology and seismic stratigraphy of the Antarctic margin, 2: 1-27.

Larter, R.D., 2007. Margin architecture reveals the transition to the modern Antarctic ice sheet ca. 3 Ma: COMMENT AND REPLY: COMMENT. Geology, 35(1): e139-e139.

Leat, P.T. et al., 2009. Zircon U-Pb dating of Mesozoic volcanic and tectonic events in north-west Palmer Land and south-west Graham Land, Antarctica. Antarctic Science, 21(6): 633-641.

1015 Leat, P.T., Scarrow, J.H., 1994. Central volcanoes as sources for the Antarctic Peninsula Volcanic
1016 Group. Antarctic science, 6(3): 365-374.

1017 Lepp, A.P., Simkins, L.M., Anderson, J.B., Clark, R.W., Wellner, J.S., Hillenbrand, C.D., Smith,
1018 J.A., Lehrmann, A.A., Totten, R., Larter, R.D. and Hogan, K.A., 2022. Sedimentary signatures of
1019 persistent subglacial meltwater drainage from Thwaites Glacier, Antarctica. Frontiers in Earth
1020 Science, 10, p.863200.

1021 Licht, K., Dunbar, N., Andrews, J., Jennings, A., 1999. Distinguishing subglacial till and glacial
1022 marine diamictons in the western Ross Sea, Antarctica: implications for a last glacial maximum
1023 grounding line. Geological Society of America Bulletin, 111(1): 91-103.

1024 Lønne, I., 1995. Sedimentary facies and depositional architecture of ice-contact glaciomarine
1025 systems. Sedimentary Geology, 98(1-4): 13-43.

1026 Marschalek, J.W. et al., 2021. A large West Antarctic Ice Sheet explains early Neogene sea-level
1027 amplitude. Nature, 600(7889): 450-455.

1028 Matsuoka, K. et al., 2021. Quantarctica, an integrated mapping environment for Antarctica, the
1029 Southern Ocean, and sub-Antarctic islands. Environmental Modelling & Software, 140: 105015.

1030 McCarron, J., Smellie, J., 1998. Tectonic implications of fore-arc magmatism and generation of
1031 high-magnesian andesites: Alexander Island, Antarctica. Journal of the Geological Society,
1032 155(2): 269-280.

1033 McCave, I., Andrews, J., 2019. Distinguishing current effects in sediments delivered to the ocean
1034 by ice. I. Principles, methods and examples. Quaternary Science Reviews, 212: 92-107.

1035 McKay, R. et al., 2012. Antarctic and Southern Ocean influences on Late Pliocene global
1036 cooling. Proceedings of the National Academy of Sciences, 109(17): 6423-6428.

1037 McLennan, S., Hemming, S., McDaniel, D., Hanson, G., 1993. Geochemical approaches to
1038 sedimentation, provenance, and tectonics.

1039 Murray, R., Miller, D.J., Kryc, K., 2000. Analysis of major and trace elements in rocks,
1040 sediments, and interstitial waters by inductively coupled plasma–atomic emission spectrometry
1041 (ICP-AES).

Naish, T. et al., 2009. Obliquity-paced Pliocene West Antarctic ice sheet oscillations. Nature, 458(7236): 322-328.

O'Brien, P., Goodwin, I., Forsberg, C.-F., Cooper, A.K., Whitehead, J., 2007. Late Neogene ice drainage changes in Prydz Bay, East Antarctica and the interaction of Antarctic ice sheet evolution and climate. Palaeogeography, Palaeoclimatology, Palaeoecology, 245(3-4): 390-410.

Orejola, N., Passchier, S., Expedition, I., 2014. Sedimentology of lower Pliocene to upper Pleistocene diamictons from IODP site U1358, Wilkes Land margin, and implications for East Antarctic Ice Sheet dynamics. Antarctic Science, 26(2): 183-192.

Passchier, S., 2025. Standard operating procedures for the laser particle size analysis of terrigenous sediments and soils. *Department of Earth and Environmental Studies Faculty Scholarship and Creative Works*. 723. https://digitalcommons.montclair.edu/earth-environ-studies-facpubs/723

Passchier, S., O'Brien, P.E., Damuth, J.E., Januszczak, N., Handwerger, D.A. and Whitehead, J.M., 2003. Pliocene–Pleistocene glaciomarine sedimentation in eastern Prydz Bay and development of the Prydz trough-mouth fan, ODP Sites 1166 and 1167, East Antarctica. Marine Geology, 199(3-4): 279-305.

Passchier, S., Laban, C., Mesdag, C.S. and Rijsdijk, K.F., 2010. Subglacial bed conditions during Late Pleistocene glaciations and their impact on ice dynamics in the southern North Sea. Boreas, 39(3): 633-647.

Passchier, S. et al., 2025. West Antarctic ice retreat and paleoceanography in the Amundsen Sea in the warm early Pliocene. Nature Communications, 16(1): 5609.

Powell, R.D., Molnia, B.F., 1989. Glacimarine sedimentary processes, facies and morphology of the south-southeast Alaska shelf and fjords. Marine Geology, 85(2-4): 359-390.

Pritchard, H. et al., 2012. Antarctic ice-sheet loss driven by basal melting of ice shelves. Nature, 484(7395): 502-505.

Pritchard, H.D., Vaughan, D.G., 2007. Widespread acceleration of tidewater glaciers on the Antarctic Peninsula. Journal of Geophysical Research: Earth Surface, 112(F3).

Prothro, L.O., Simkins, L.M., Majewski, W., Anderson, J.B., 2018. Glacial retreat patterns and processes determined from integrated sedimentology and geomorphology records. Marine Geology, 395: 104-119.

Rebesco, M., Camerlenghi, A., Geletti, R., Canals, M., 2006. Margin architecture reveals the transition to the modern Antarctic ice sheet ca. 3 Ma. Geology, 34(4): 301-304.

Reinardy, B.T. et al., 2015. Repeated advance and retreat of the East Antarctic Ice Sheet on the continental shelf during the early Pliocene warm period. Palaeogeography, Palaeoclimatology, Palaeoecology, 422: 65-84.

Riley, T.R., Flowerdew, M.J., Whitehouse, M.J., 2012. Chrono-and lithostratigraphy of a Mesozoic–Tertiary fore-to intra-arc basin: Adelaide Island, Antarctic Peninsula. Geological Magazine, 149(5): 768-782.

Riley, T.R., Macdonald, D.I., Cantrill, D.J., Crame, J.A., Curtis, M.L., 2025. The geology of Alexander Island (Antarctic Peninsula): a new 1: 500 000 geological map. Antarctic Science: 1-20.

Riley, T.R. et al., 2023. Evolution of an accretionary complex (LeMay Group) and terrane translation in the Antarctic Peninsula. Tectonics, 42(2): e2022TC007578.

Scambos, T.A., Bohlander, J., Shuman, C.A., Skvarca, P., 2004. Glacier acceleration and thinning after ice shelf collapse in the Larsen B embayment, Antarctica. Geophysical Research Letters, 31(18).

Shipboard Scientific Party, 1999. Site 1097. In Barker, P.F., Camerlenghi, A., Acton, G.D., et al., Proc. ODP, Init. Repts., 178: College Station, TX (Ocean Drilling Program), 1–66. doi:10.2973/odp.proc.ir.178.107.1999

Smellie, J.L., Haywood, A.M., Hillenbrand, C.-D., Lunt, D.J., Valdes, P.J., 2009. Nature of the Antarctic Peninsula Ice Sheet during the Pliocene: Geological evidence and modelling results compared. Earth-Science Reviews, 94(1-4): 79-94.

Smith, C.G., 1987. The geology of parts of the west coast of Palmer Land, 112. British Antarctic Survey.

Smith, J.A. et al., 2007. Oceanic and atmospheric forcing of early Holocene ice shelf retreat, George VI Ice Shelf, Antarctica Peninsula. Quaternary Science Reviews, 26(3-4): 500-516.

Smith, J.A. et al., 2019. The marine geological imprint of Antarctic ice shelves. Nature Communications, 10(1): 5635.

Smith, B., Fricker, H.A., Gardner, A.S., Medley, B., Nilsson, J., Paolo, F.S., Holschuh, N., Adusumilli, S., Brunt, K., Csatho, B. and Harbeck, K., 2020. Pervasive ice sheet mass loss reflects competing ocean and atmosphere processes. Science, 368(6496): 1239-1242.

Tauxe, L. et al., 2012. Chronostratigraphic framework for the IODP Expedition 318 cores from the Wilkes Land Margin: Constraints for paleoceanographic reconstruction. Paleoceanography, 27(2).

Tibbett, E.J. et al., 2021. Late Eocene record of hydrology and temperature from Prydz Bay, East Antarctica. Paleoceanography and Paleoclimatology, 36(4): e2020PA004204.

Tierney, J.E. et al., 2025. Pliocene warmth and patterns of climate change inferred from paleoclimate data assimilation. AGU Advances, 6(1): e2024AV001356.

Uenzelmann-Neben, G., 2006. Depositional patterns at Drift 7, Antarctic Peninsula: Along-slope versus down-slope sediment transport as indicators for oceanic currents and climatic conditions. Marine Geology, 233(1-4): 49-62.

Vaughan, D.G., 2006. Recent trends in melting conditions on the Antarctic Peninsula and their implications for ice-sheet mass balance and sea level. Arctic, Antarctic, and Alpine Research, 38(1): 147-152.

Wareham, C.D., Millar, I.L., Vaughan, A.P., 1997. The generation of sodic granite magmas, western Palmer Land, Antarctic Peninsula. Contributions to Mineralogy and Petrology, 128(1): 81-96.

Westerhold, T. et al., 2020. An astronomically dated record of Earth's climate and its predictability over the last 66 million years. science, 369(6509): 1383-1387.

Whitehead, J., Wotherspoon, S., Bohaty, S., 2005. Minimal Antarctic sea ice during the Pliocene. Geology, 33(2): 137-140.

1123 Whitehead, J.M., Bohaty, S.M., 2003. Pliocene summer sea surface temperature reconstruction
1124 using silicoflagellates from Southern Ocean ODP Site 1165. Paleoceanography, 18(3).

1125 Willan, R.C., 2003. Provenance of Triassic-Cretaceous sandstones in the Antarctic Peninsula:
1126 implications for terrane models during Gondwana breakup. Journal of Sedimentary Research,
1127 73(6): 1062-1077.

1128 Winter, D., and Iwai, M., 2002. Data report: Neogene diatom biostratigraphy, Antarctic Peninsula
1129 Pacific margin, ODP Leg 178 rise sites. In Barker, P.F., Camerlenghi, A., Acton, G.D., and
1130 Ramsay, A.T.S. (Eds.), Proc. ODP, Sci. Results, 178: College Station, TX (Ocean Drilling
1131 Program), 1–25. doi:10.2973/odp.proc.sr.178.230.2002

1132

FIGURES

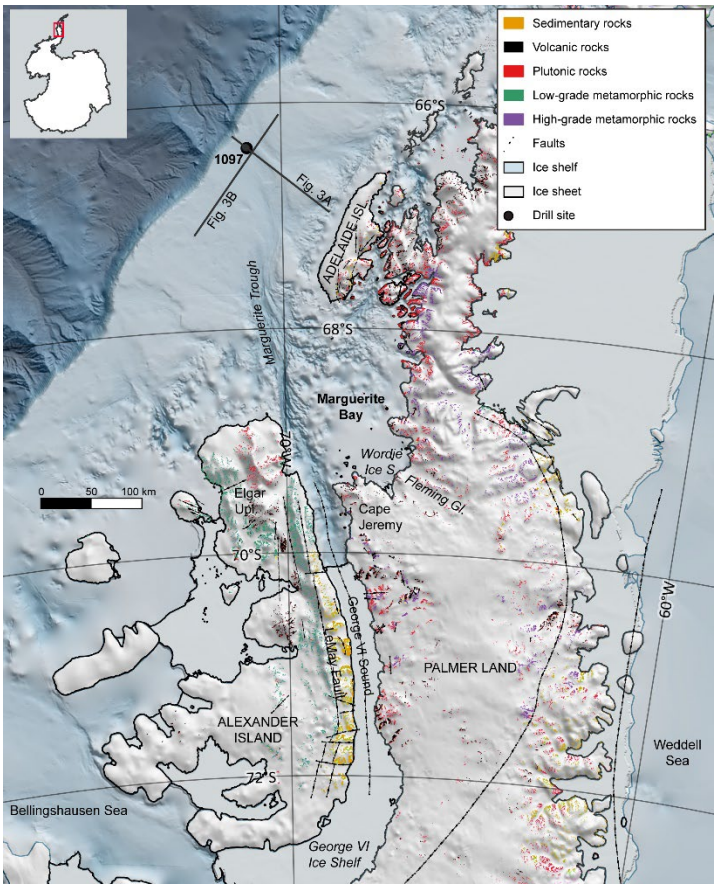

Figure 1. Location map of the study area and Site 1097 with topography and bathymetry from Dorschel et al. (2022) and bedrock geology of ice-free areas after Cox et al. (2023). Approximate locations of the interpreted seismic profiles depicted in Figure 3 are also indicated. The map was created in QGIS 4.0 using the Quantartica package (Matsuoka et al., 2021).

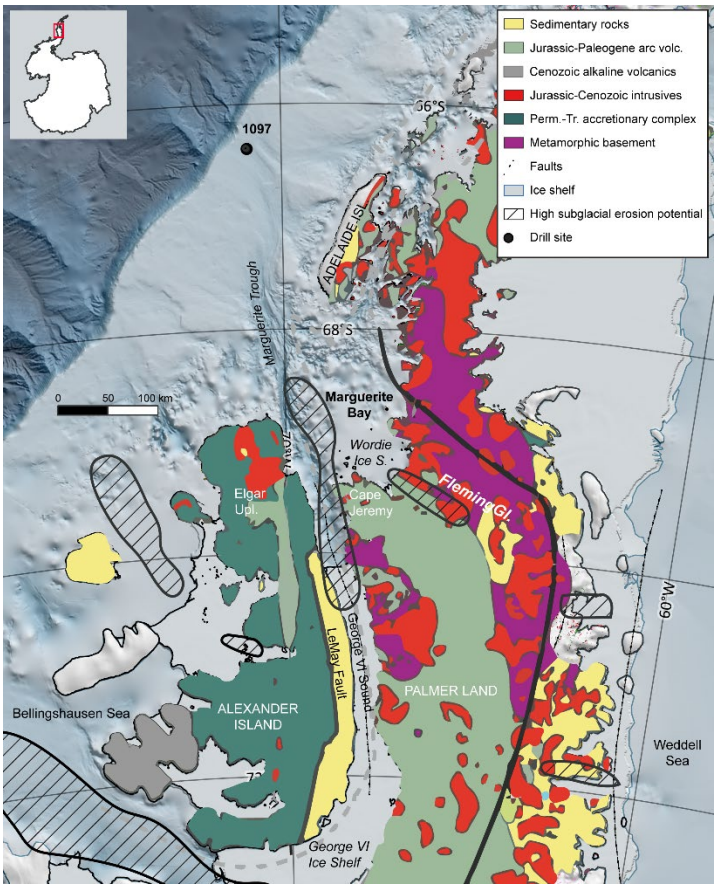

Figure 2. Geological map of the study area after Burton-Johnson and Riley (2015) with bathymetry from Dorschel et al. (2022). Subglacial erosion potential is mapped after the LGM and deglacial model output in Golledge (2014). The map was created in QGIS 4.0 using the Quantartica package (Matsuoka et al., 2021).

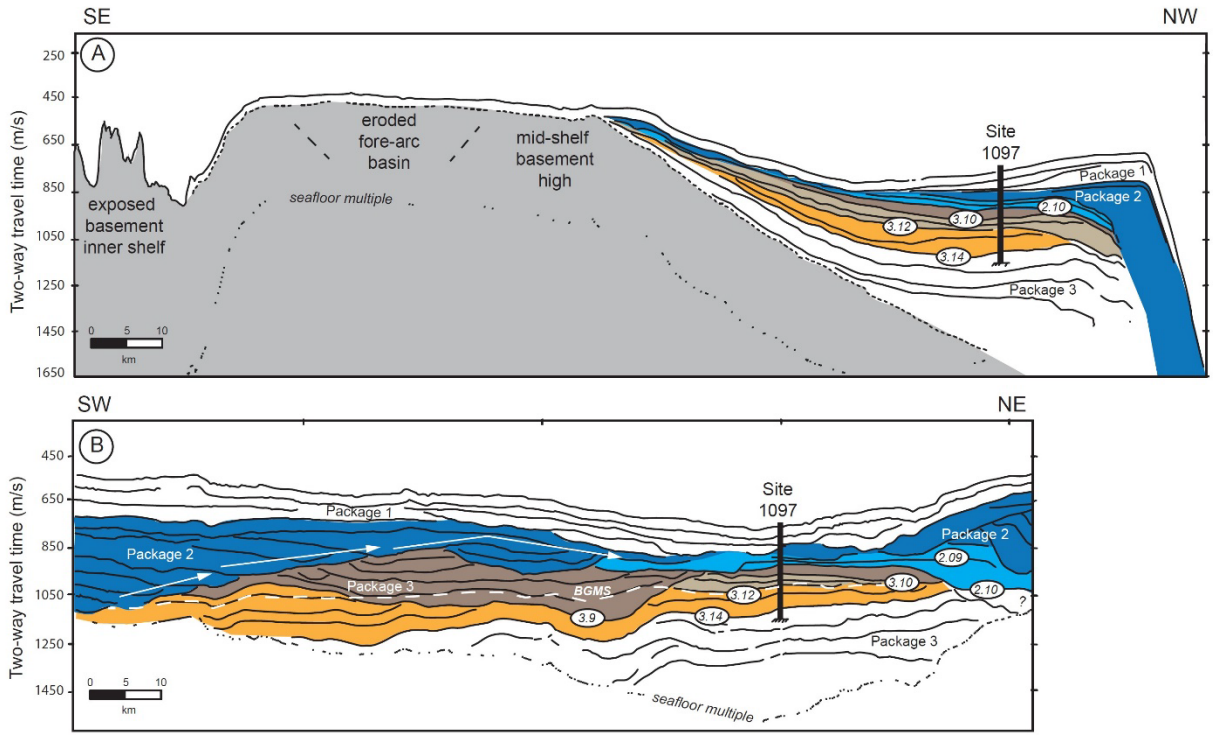

Figure 3. Interpretation of seismic line segments running from A) inner continental shelf to continental slope and B) across the shelf parallel to the shelf edge. Map locations of the lines can be found in Figure 1. The black reflector tracing and labeling is from Bart and Iwai (2012). The white dashed line labeled BGMS and the arrows in the lower panel are derived from an interpretation of the same line in Hernández-Molina et al. (2017). BGMS stands for "base of glacial margin sequences" and the arrows indicate the interpreted eastward migration of the paleo-trough of Hernández-Molina et al. (2017). All traces were scaled to the 40x vertical exaggeration used in Bart and Iwai (2012).

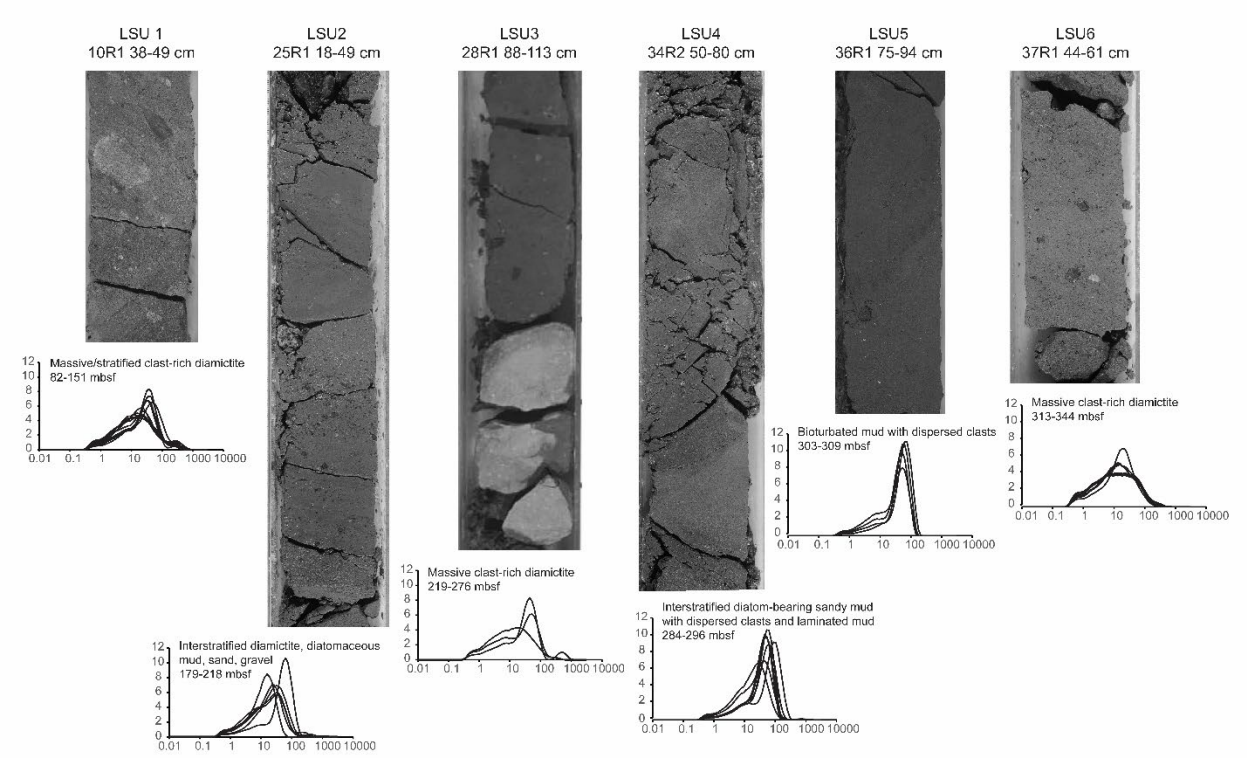

Figure 4. Particle size distributions and core photos for each of the new Lithostratigraphic Units (LSUs) defined at Site 1097. See the text for descriptions of the LSUs. Core images from Shipboard Scientific Party (1999).

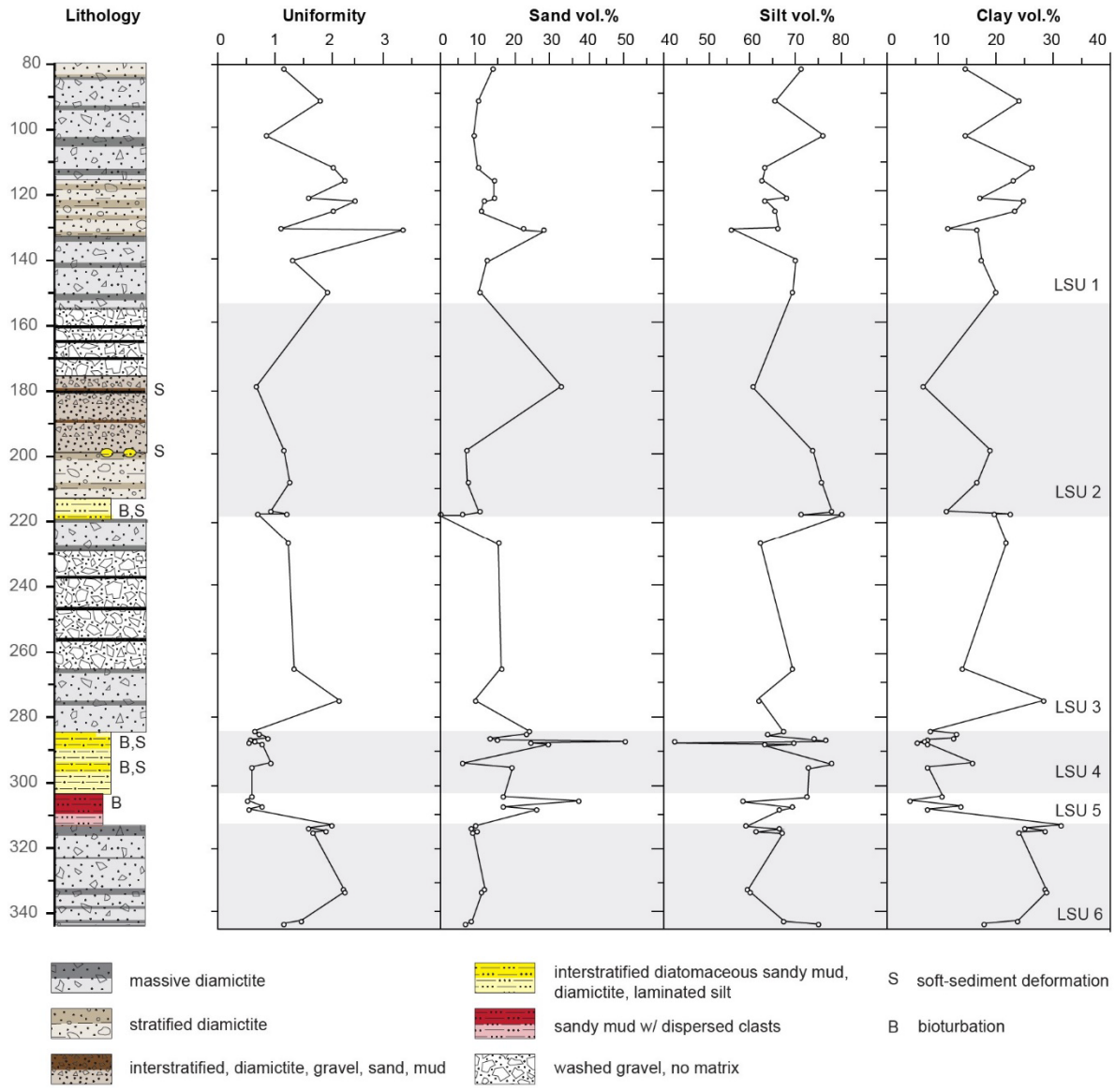

Figure 5. Lithological log based on interpretations of shipboard core description and core images (Shipboard Scientific party, 1999), and downcore distributions of grain-size classes in the ~82-343 m interval at Site 1097. Uniformity is defined as the D60/D10 ratio and is a measure of the sorting of the sediment (0.01-3000 µm), with lower values (~1) indicating well-sorted materials and higher values > 2 indicating poorly sorted materials.

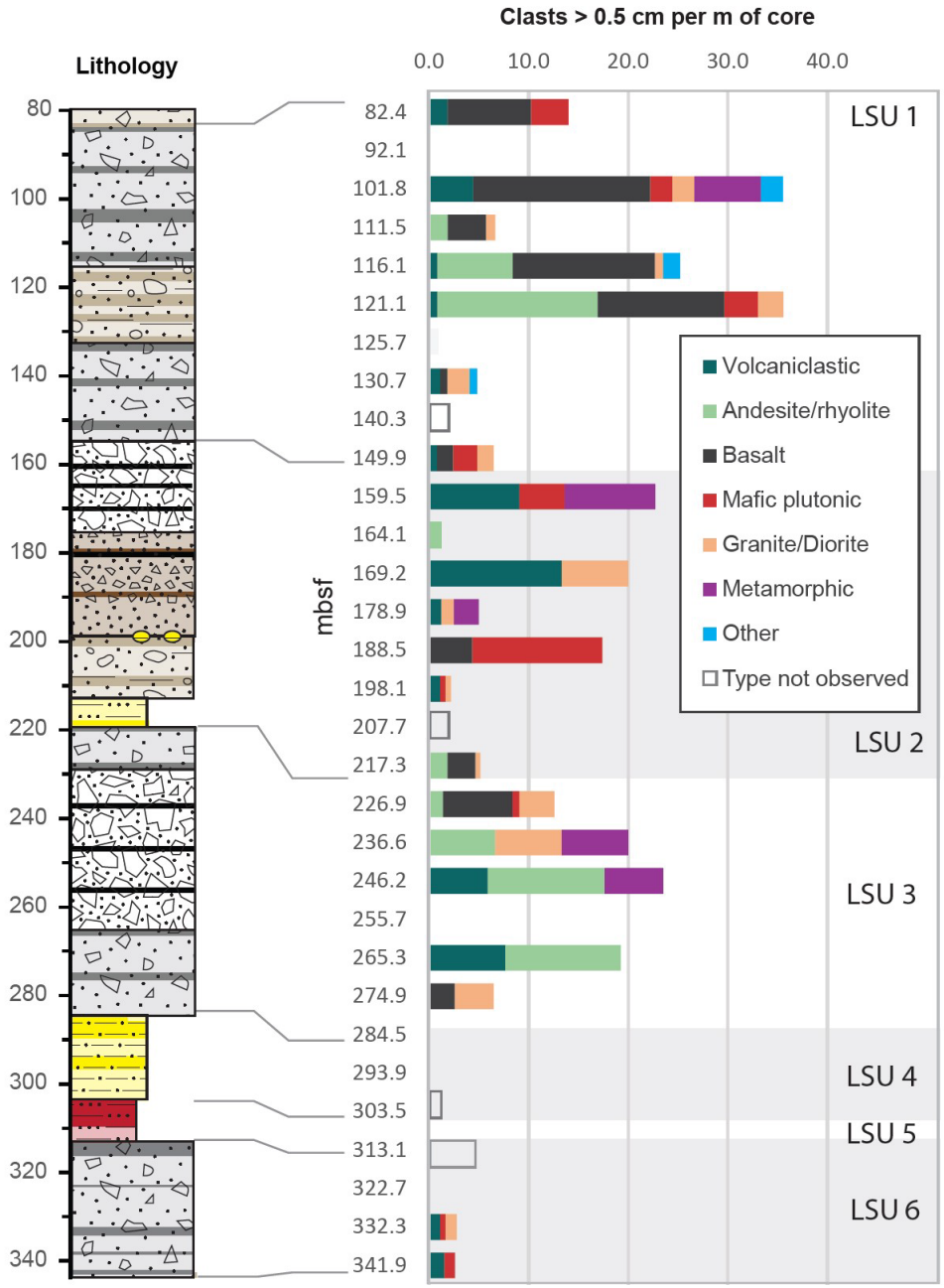

1163

1164 Figure 6. Clast petrology for clasts more than 0.5 cm in diameter normalized per meter of core
1165 recovered. Data source: Shipboard Scientific Party (1999).

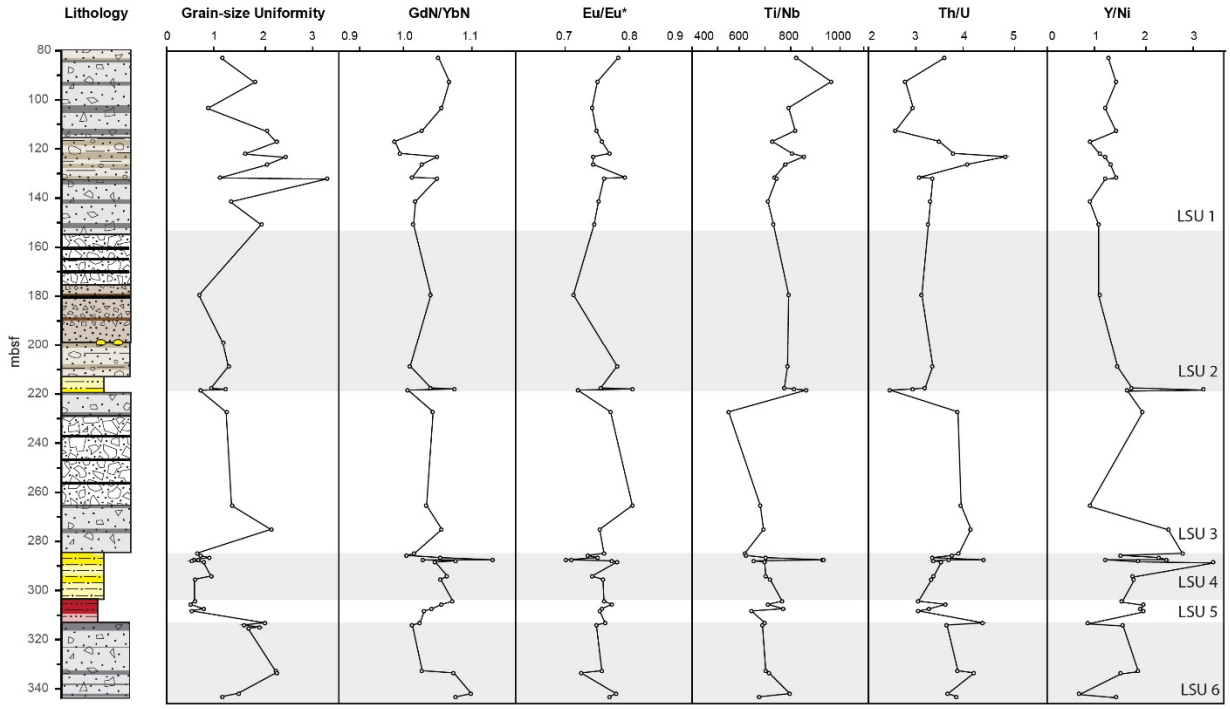

Figure 7. Down core distributions of trace and rare earth elemental ratios indicating changes in detrital mineral composition. The legend for the lithological log is in Figure 5.

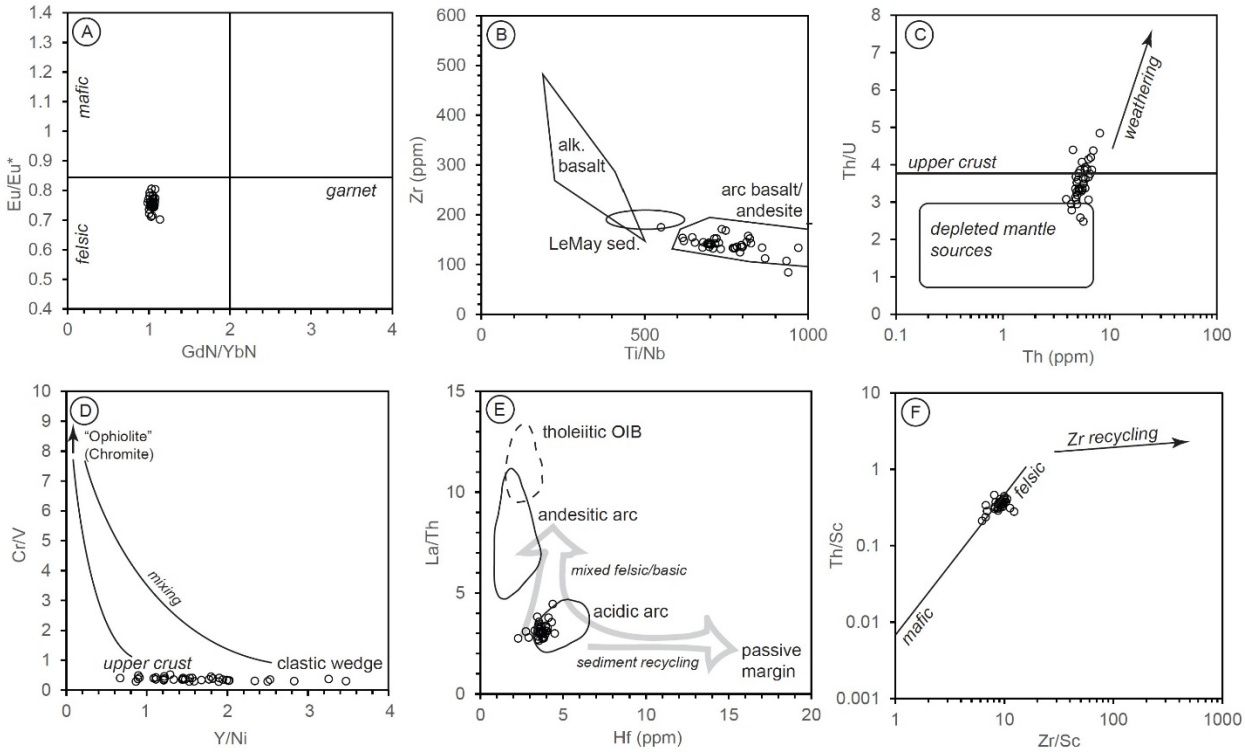

Figure 8. Biplots for trace and rare earth elemental ratios with interpretations of detrital provenance according to McLennan et al. (1993), Floyd and Leveridge (1987) and Bonjour and Dabard (1991).

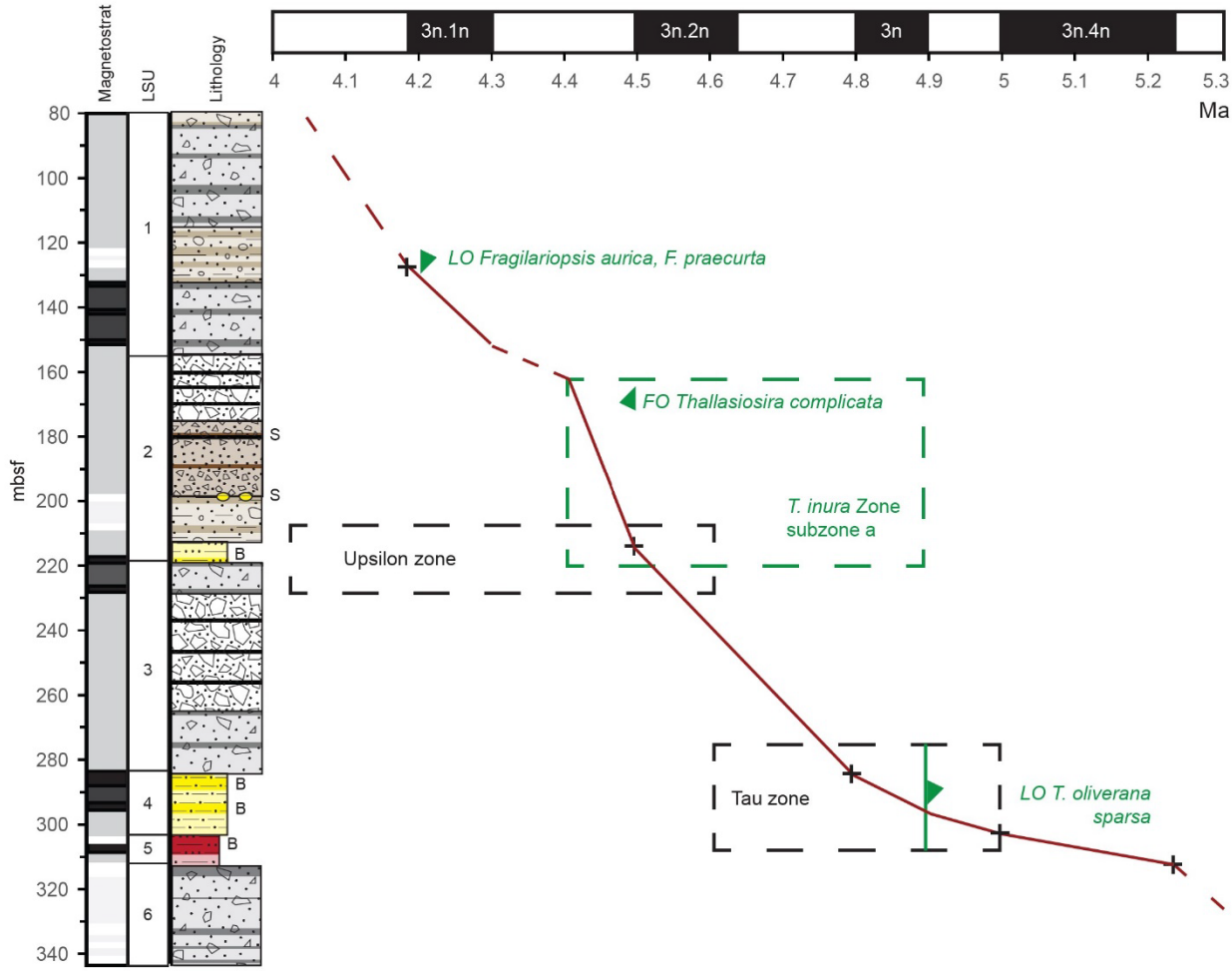

Figure 9. Age model for Site 1097 using updated ranges for microfossil zonations from McKay et al (2019) and Kato et al. (2024) with an interpretation of the sparse shipboard magnetostratigraphy. Data from Shipboard Scientific Party (1999) and Iwai and Winter (2002).

1179 TABLE

Sedimentology					Provenance			
Seismic Pack.	**1097 LSU**	**Facies**	**Environment**	**Clast petrology**	**Geo-chemistry**	**Source rocks**	**Bio-magneto-stratigraphy**	**Age (Ma)**
2	1	Dm, Ds	Subglacial, polar glaciomarine	basalt, andesite/rhyolite, metamorphic, mafic plutonic	Ti/Nb >>>, Th/U extremes	mafic, sedim., NW Palmer Land, George VI Sound	*LO F. Aurica*, *F. praecurta*, 3n.1n	4.3-4.1
3	2	Ds, M, S, G	Ice-proximal meltwater-rich and ice distal, gravity flow	volcaniclastic, mafic plutonic, metamorphic, granite/diorite	Ti/Nb >>, Y/Ni <<, Th/U <<, $^{39}Ar/^{40}Ar$ 118-142 Ma	mafic, NW Palmer Land, Fleming Glacier	*T. Inura* subzone b	4.5-4.3
BGMS	3	Dm, Ds	Subglacial, subpolar glaciomarine	andesite/rhyolite, volcaniclastic, metamorphic, granite/diorite	Ti/Nb <<, Th/U >>, Y/Ni >>	NW Palmer Land, Alexander Isl., mid-shelf high fore-arc basin	Tau Zone to Upsilon Zone, *T. Inura* subzone b	4.8-4.5
3	4	M	Ice-distal hemipelagic	N.D. clast-poor	Y/Ni >>, Gd/Yb >>	felsic coastal Alexander, Adelaide Isl., Marguerite Bay	Tau Zone, Chron 3n.3n	5.0-4.8
3	5	M	Ice-distal hemipelagic	N.D. clast-poor	Y/Ni >>, Gd/Yb >>	felsic coastal Alexander, Adelaide Isl., Marguerite Bay	*LO T. Oliverana sparsa*, Tau Zone, top Chron 3n.4n	5.2-5.0
3	6	Dm, Ds	Ice-proximal glaciomarine	volcaniclastic, mafic plutonic, granite/diorite	Th/U >>, Gd/Yb <<	Alexander, Adelaide Island, Marguerite Bay	Below top Chron 3n.4n	> 5.2

1180

1181 Table 1. Summary table of interpretations of sedimentology, provenance and chronostratigraphy
1182 of Site 1097.